The insulin receptor adaptor IRS2 is an APC/C substrate that promotes cell cycle protein expression and a robust spindle assembly checkpoint

Sandhya Manohar[1], Qing Yu[1], Steven P. Gygi[1], Randall W. King[1,2*]

1. Department of Cell Biology, Harvard Medical School, Boston, Massachusetts 02115, USA.
2. Lead contact

* Correspondence: randy_king@hms.harvard.edu

Summary

Insulin receptor substrate 2 (IRS2) is an essential adaptor that mediates signaling downstream of the insulin receptor and other receptor tyrosine kinases. Transduction through IRS2-dependent pathways is important for coordinating metabolic homeostasis, and dysregulation of IRS2 causes systemic insulin signaling defects. Despite the importance of maintaining proper IRS2 abundance, little is known about what factors mediate its protein stability. We conducted an unbiased proteomic screen to uncover novel substrates of the Anaphase Promoting Complex/Cyclosome (APC/C), a ubiquitin ligase that controls the abundance of key cell cycle regulators. Surprisingly, we found that IRS2 levels are regulated by APC/C activity and that IRS2 is a direct APC/C target in G_1. Consistent with the APC/C's role in degrading cell cycle regulators, we find that IRS2-null cells are deficient in proteins involved in cell cycle progression and display spindle assembly checkpoint defects during M-phase. Together, these findings reveal a new pathway for IRS2 turnover and indicate that IRS2 is a critical component of the cell cycle control system in addition to acting as an essential metabolic regulator.

Keywords

Anaphase-Promoting Complex/Cyclosome; ubiquitin; cell cycle; insulin signaling pathway; G_1

Introduction

The insulin and insulin-like growth factor 1 receptors (IR/IGF1R) are receptor tyrosine kinases that control metabolism, differentiation, and growth. Upon ligand binding at the cell surface, the activated IR/IGF1R undergoes a conformational change that allows it to auto-phosphorylate tyrosine residues on its cytoplasmic subunits (Haeusler et al., 2017). This facilitates the recruitment and phosphorylation of insulin receptor substrate (IRS) proteins, which serve as scaffolds to initiate downstream signaling (Copps and White, 2012). Two major pathways that are stimulated by this cascade are the PI3K-AKT and Ras-Raf-MAPK pathways, which coordinate metabolic homeostasis and growth, among other functions (Haeusler et al., 2017).

The most physiologically important and ubiquitously expressed IRS proteins are IRS1 and IRS2. Though IRS1 and IRS2 share similar structural and functional features, they have complementary roles and expression patterns that depend on tissue type and physiological state (Haeusler et al., 2017). These differences are illustrated by divergent phenotypes in knockout mice: whereas IRS1 knockout mice exhibit insulin resistance that is compensated by increased pancreatic β cell mass, IRS2 knockout mice exhibit β cell failure and resultant diabetes (Lavin et al., 2016). Distinct roles for IRS1 and IRS2 can also be observed within the same tissue. For example, in skeletal muscle, IRS1 is required for glucose uptake and metabolism, whereas IRS2 is important for lipid uptake and metabolism (Bouzakri et al., 2006; Long et al., 2011). Furthermore, recent work has shown that the ratio of IRS1 to IRS2 is important for hepatic glucose metabolism (Besse-Patin et al., 2019). Thus, maintaining proper IRS1 and IRS2 levels is critical for systemic and cellular homeostasis.

The ubiquitin-mediated proteolysis of IRS proteins is important for restraining signaling through the IR/IGF1R. For example, both IRS proteins are targeted for proteasomal destruction following persistent insulin or IGF1 stimulation in a negative feedback loop that attenuates PI3K-AKT signaling (Copps and White, 2012; Scheufele et al., 2014). In mice, removal of a ubiquitin ligase that is responsible for IGF1-induced degradation of IRS1 enhances insulin sensitivity and increases plasma glucose clearance (Scheufele et al., 2014). Though several ubiquitin ligases have been reported to control IRS1's proteasome-dependent degradation (Nakao et al., 2009; Rui et al., 2002; Shi et

al., 2011; Xu et al., 2008; Yi et al., 2013), only SOCS1/3 have been implicated in driving IRS2 turnover (Rui et al., 2002). This is an intriguing disparity because hepatic IRS1 remains stable between fasting and feeding whereas IRS2 levels drop after feeding (Kubota et al., 2008), suggesting that IRS2 is less stable than IRS1 in some physiological contexts. Because SOCS1/3 also targets IRS1, there are no reports of ubiquitin ligases that target IRS2 but not IRS1, leaving a gap in our knowledge of how IRS1 and IRS2 are differentially regulated by the ubiquitin proteasome system.

The Anaphase-Promoting Complex/Cyclosome (APC/C) is a 1.2 mDa ubiquitin ligase that targets key cell cycle related proteins for destruction by the proteasome (Alfieri et al., 2017; Chang and Barford, 2014). To transfer ubiquitin to its substrates, the APC/C works with one of two co-activators: Cdc20 during M-phase or Cdh1 during G_1. These co-activators stimulate the catalytic activity of the APC/C and facilitate substrate recognition. APC/C^{Cdc20} and APC/C^{Cdh1} recognize substrates via short degron motifs in unstructured protein regions called destruction boxes (D-boxes) and KEN-boxes. An additional degron, called the ABBA motif, is used by APC/C^{Cdc20} only (Alfieri et al., 2017; Chang and Barford, 2014; Davey and Morgan, 2016).

To probe the substrate landscape of the APC/C, we conducted an unbiased proteomic screen by acutely blocking APC/C^{Cdh1} activity with small molecule APC/C inhibitors (apcin and proTAME) (Sackton et al., 2014; Zeng et al., 2010) in G_1 cells. Using this approach, we uncovered diverse putative APC/C^{Cdh1} substrates, including IRS2. We demonstrate that IRS2, but not IRS1, is a direct target of APC/C^{Cdh1}, thereby establishing a novel mode by which IRS1 and IRS2 are differentially regulated. Using IRS2 knockout cell lines, we show that IRS2 is important for the expression of proteins involved in cell cycle progression. We further show that genetic deletion of IRS2 perturbs spindle assembly checkpoint function. Taken together, these data establish a role for IRS2 in normal cell cycle progression, revealing new connections between an essential component of the growth factor signaling network and cell cycle regulation.

Results

Chemical proteomics reveals proteins whose abundances are APC/C^{Cdh1} regulated

93 To identify novel substrates and pathways regulated by APC/C^{Cdh1}, we designed
94 an experiment that coupled small molecule inhibition of the APC/C in G_1 cells to high
95 resolution tandem mass tag (TMT)-based quantitative proteomics (**Figure 1A**). Blocking
96 Cdk4/6 activity inhibits Rb phosphorylation, causing cells to arrest at the G_1 restriction
97 point (Ezhevsky et al., 1997). Thus, to generate a homogeneous population of G_1 cells,
98 we treated asynchronous hTERT-RPE1 cells bearing fluorescent ubiquitination-based
99 cell cycle indicator (FUCCI) constructs (Sakaue-Sawano et al., 2008) with the Cdk4/6
100 inhibitor palbociclib. Following G_1 arrest, cells were acutely treated with a combination of
101 APC/C inhibitors (6 μM proTAME + 50 μM apcin) or vehicle (DMSO) for 8 hours. Cells
102 were then collected for proteomic analysis with the expectation that APC/C-regulated
103 proteins would be stabilized in cells treated with APC/C inhibitors compared to control
104 cells (**Figure 1A**). The combined use of proTAME and apcin results in robust inhibition of
105 the APC/C (Sackton et al., 2014), which guided our decision to use this treatment scheme.
106 Moreover, this scheme was designed to specifically identify APC/C^{Cdh1} substrates rather
107 than APC/C^{Cdc20} substrates since APC/C^{Cdh1} degrades Cdc20 during G_1 phase (Prinz et
108 al., 1998). Illustrating this point, Cdc20 was undetectable in G_1 palbociclib-arrested cells
109 (**Figure 1B**).
110 The experimental approach outlined in **Figure 1A** was validated using the FUCCI
111 reporter system. This system relies on the expression of two stably integrated fluorescent
112 fusion proteins—mAG1-geminin (1-110) and mCherry-Cdt1 (30-120)—to monitor the
113 activity of endogenous cell cycle-related ubiquitin ligases APC/C^{Cdh1} and SCF^{Skp2},
114 respectively (Sakaue-Sawano et al., 2008). As expected, cells treated with palbociclib lost
115 mAG1-geminin (1-110) protein expression over time due to APC/C^{Cdh1} activity while
116 mCherry-Cdt1 (30-120) was stabilized, indicating G_1 arrest (**Figures S1A-S1B**). The
117 addition of APC/C inhibitors in palbociclib-arrested cells rescued mAG1-geminin (1-110)
118 levels (**Figures S1C-S1D**), confirming that this workflow stabilizes APC/C targets.
119 Using TMT-coupled quantitative proteomics, we identified and quantified relative
120 abundances for ~8000 human proteins in G_1-arrested cells treated with or without APC/C
121 inhibitors in biological triplicate (**Supplementary Table S1**). Notably, we detected 38
122 previously reported APC/C substrates in our dataset (**Figures 1C-1D; Supplementary
123 Table S2).** Of these, 22 increased significantly ($p < 0.05$) under conditions of APC/C

124 inhibition. As an internal control, we detected a significant increase (p = 3.2 x 10^{-5}) in the
125 abundance of peptides derived from the N-terminal 110 amino acids of geminin (GMNN).
126 These residues are shared with the mAG1-geminin (1-110) reporter expressed in this cell
127 line, confirming earlier fluorescence-based validation of our experimental system.

128 While the majority of the previously reported APC/C^{Cdh1} substrates that were
129 quantified in our G_1 proteomic experiment were stabilized following APC/C inhibition,
130 some remained constant. There are several possible explanations for this result. First, for
131 proteins that were identified based on a small number of peptides, inadequate
132 quantification may have resulted in inaccurate abundance assignments. Second, some
133 substrates may be APC/C^{Cdh1}-accessible only under conditions or in tissue types that
134 were not well modeled by the experimental parameters that we used. Third, some
135 proteins (e.g. FBXW5, ZC3HC1) (Klitzing et al., 2011; Puklowski et al., 2011) were
136 proposed to be APC/C^{Cdh1} substrates based on results obtained in Cdh1 overexpression
137 systems, indicating that APC/C^{Cdh1} activity may be sufficient but not necessary to control
138 their levels.

139 Of the 38 previously reported APC/C substrates that we identified, the median fold
140 change under APC/C inhibition compared to DMSO was 1.147. Based on this, to identify
141 new APC/C substrates, we screened for proteins that: (1) had a fold change ≥1.147 under
142 APC/C inhibition, (2) were identified and quantified based on >1 peptide, and (3) had a p-
143 value < 0.05 across the three biological replicates measured in this experiment. This
144 narrowed our analysis to a subset of 204 proteins (**Supplementary Table S3**). Because
145 the APC/C recognizes substrates based on D-box motifs (RxxL or the extended motif
146 RxxLxxxxN) and KEN-box motifs (KEN), we used the SLiMSearch (Short Linear Motif
147 Search) degron prediction tool(Davey and Morgan, 2016; Krystkowiak and Davey, 2017)
148 to scan this 204-protein subset for proteins that contain these sequences. In order to
149 classify a putative D- or KEN-box sequence as a probable physiological degron, we
150 applied the following restrictions on the SLiMSearch (Krystkowiak and Davey, 2017)
151 parameters: (1) similarity score ≥ 0.75; (2) consensus similarity is medium or high; (3)
152 disorder score ≥ 0.4; (4) the putative degron must be intracellular and exist on a non-
153 secreted protein. These cutoffs were determined based on those met by previously
154 validated APC/C substrates (including those not identified in our dataset) and by the

155 physical restriction that APC/C activity occurs within the cell. Based on these thresholds,
156 our analysis identified 26 proteins as potential D- and KEN-box containing APC/C^{Cdh1}
157 substrates (**Table 1, Figure 1D**). Of these 26 proteins, 11 have previously been reported
158 as direct APC/C substrates, validating internally that this analysis was useful for
159 identifying APC/C substrates.
160
161 *IRS2 levels are controlled by Cdh1 in a proteasome-dependent manner*
162 Examining our 26-protein putative substrate list, we focused our attention on
163 IRS2—one of two major adaptors that promotes signaling through the insulin and insulin-
164 like growth factor 1 receptors (IR/IGF1R). Using conditions identical to those under which
165 the proteomics experiment was conducted, we validated that IRS2 was upregulated at
166 the protein level under APC/C inhibition in G_1-arrested RPE1 cells by immunoblot (**Figure**
167 **2A**). Seeking to further validate this result in a distinct physiological context, we asked
168 whether APC/C inhibition in terminally differentiated C_2C_{12} myotubes also increases IRS2
169 protein abundance. C_2C_{12} myoblasts easily differentiate into multinucleated myotubes
170 following serum withdrawal and supplementation with growth factors (**Figures S2A-S2B**).
171 To validate that the APC/C is active in this system, we transfected C_2C_{12} myoblasts with
172 a model APC/C substrate (N-terminal fragment of cyclin B1 fused to EGFP; NT-CycB-
173 GFP), allowed cells to differentiate into myotubes, and found that APC/C inhibition
174 stabilized NT-CycB-GFP (**Figure S2C**). Similarly, we found that acute APC/C inhibition in
175 myotubes also resulted in an accumulation of IRS2 protein (**Figure 2B**), thereby validating
176 this finding from our G_1 experiment in RPE1 cells in an independent system.
177 To exclude the possibility that the change in IRS2 abundance that we observed
178 following APC/C inhibition was due to off-target effects of the small molecule APC/C
179 inhibitors, we depleted Cdh1 using RNAi to block APC/C^{Cdh1} activity in RPE1, C_2C_{12}, and
180 HeLa cells. In all three cell lines, we found that Cdh1 knockdown caused an accumulation
181 of endogenous IRS2 compared to control-transfected cells (**Figure 2C-2E**).
182 We next sought to confirm that the increase in IRS2 protein observed under APC/C
183 inhibition was due to impaired targeting of IRS2 to the proteasome. To test this, we
184 arrested RPE1 cells in G_1 using palbociclib and acutely treated them with APC/C inhibitors
185 and/or a proteasome inhibitor (MG132) for 8 hours. This experiment revealed that APC/C

186 inhibition or proteasome inhibition each resulted in an accumulation of IRS2 (**Figure 2F**).
187 Notably, co-inhibition of the APC/C and the proteasome did not result in additional
188 stabilization of IRS2, indicating that the increase in IRS2 we observed under APC/C
189 inhibition was solely a consequence of its impaired ubiquitination and proteasomal
190 degradation.
191
192 *IRS2 levels and phosphorylation fluctuate in a cell-cycle dependent manner*
193 To test whether IRS2 levels fluctuate during the cell cycle as expected for an
194 APC/C substrate, we synchronized HeLa cells in early S-phase by double thymidine block
195 and tracked IRS2 protein abundance leading into mitotic entry by immunoblot (**Figure**
196 **3A**). As is typical for known APC/C substrates, IRS2 levels correlated with cyclin B1
197 abundance and APC3 phosphorylation. To assess IRS2 levels at mitotic exit, we
198 thymidine-nocodazole synchronized HeLa cells, released them into prometaphase, and
199 tracked IRS2's abundance through mitotic exit (**Figure 3B**). Again, IRS2 protein
200 abundance correlated with cyclin B1 levels and APC3 phosphorylation. The same
201 behavior was observed in RPE1 cells that were synchronized in late G_2 by RO3306
202 treatment (Cdk1 inhibition) and tracked over the course of progression through M-phase
203 and into G_1 (**Figure 3C**). Based on these data, we conclude that IRS2 protein levels
204 fluctuate in a cell cycle dependent manner that is consistent with other known APC/C
205 substrates.
206 In agreement with previous reports of mitotic phosphorylation of IRS2 by Plk1
207 (Chen et al., 2015), our cell cycle analysis experiments revealed that IRS2 displays a
208 marked electrophoretic mobility shift consistent with mitotic phosphorylation. This may
209 owe, at least in part, to Cdk1 activity given that HeLa cells released from a double
210 thymidine block into Cdk1 inhibitor RO3306 did not display an observable shift in IRS2
211 mobility as compared to those released into control (DMSO) treatment (**Figure S3**). IRS2
212 abundance still peaked normally at this time point in the presence of RO3306, suggesting
213 that the increase in IRS2 abundance was not dependent on Cdk1 activity. Together, these
214 results support previous findings (Chen et al., 2015) that IRS2 is subject to cell-cycle
215 dependent phosphorylation and that its abundance peaks in M-phase and falls in early
216 G_1 in multiple cell lines.

217 *Cdh1 control of IRS2 degradation depends on an IRS2 D-box motif*

218 Based on its SLiMSearch prediction, IRS2 contains four minimal D-box motifs
219 (RxxL), one extended D-box motif (RxxLxxxxN) and no KEN-box motifs. Of the four
220 minimal D-box motifs, none bear strong consensus similarity to previously validated D-
221 box motifs, and one exists in a highly structured region of the protein (Krystkowiak and
222 Davey, 2017). Because of its high SLiMSearch parameter scores (**Table 1**), we focused
223 our efforts on determining whether the extended D-box motif located in the C-terminal
224 third of IRS2 is required for its APC/C^{Cdh1} dependent stability. IRS2's extended D-box
225 (amino acids 972-980 in human IRS2) is highly conserved in placental mammals despite
226 overall divergence in much of the C-terminus (**Figure 4A**), suggesting that this sequence
227 likely has a conserved function.

228 To test whether IRS2's full D-box is relevant for its Cdh1-dependent degradation,
229 we generated a mutant IRS2 construct bearing an R972A mutation (ΔD), which was
230 expected to abrogate its function as a D-box (Glotzer et al., 1991). Using RPE1 cells
231 stably expressing C-terminally HA-tagged IRS2-WT or IRS2-ΔD, we found that APC/C
232 inhibition following G_1 arrest caused accumulation of IRS2-WT but not IRS2-ΔD (**Figure**
233 **4B**). The degree of accumulation of the WT protein depended on the dose of APC/C
234 inhibitors used (**Figure S4A**). We were moreover able to repeat this result in terminally
235 differentiated C_2C_{12} myotubes that stably expressed doxycycline-inducible, C-terminally
236 HA-tagged IRS2-WT or IRS2-ΔD constructs that were treated with APC/C inhibitors
237 (**Figure 4C**).

238 To further validate the Cdh1-dependence of IRS2's D-box motif, we asked whether
239 Cdh1 knockdown by siRNA could stabilize the IRS2-ΔD protein. Using asynchronous
240 RPE1 cells stably expressing C-terminally HA-tagged IRS2-WT and IRS2-ΔD, we found
241 that Cdh1 knockdown by siRNA caused an accumulation of IRS2-WT relative to control-
242 transfected cells but not IRS2-ΔD (**Figure 4D**). This result was repeated in HeLa cells
243 stably expressing N-terminally FLAG-HA-tagged IRS2-WT and IRS2-ΔD constructs
244 subject to the same conditions (**Figure 4E**).

245 The stable cell lines described above express tagged IRS2 variants at low levels
246 comparable to the endogenous protein (**Figure S4B**), making it unlikely that the observed
247 effects were protein overexpression artifacts. Notably, IRS1 (the other primary adaptor

248 protein for the IGF1R and IR) shares 75% sequence homology with IRS2's N-terminus
249 and 35% homology with its C-terminus (Sun et al., 1995) but does not share the D-box
250 motif found in IRS2's C-terminus (**Figure 4F**). In keeping with our hypothesis that Cdh1-
251 mediated control of IRS2 is D-box dependent, IRS1 levels did not increase in G_1-arrested
252 RPE1 cells treated with APC/C inhibitors as measured by either mass spectrometry
253 (**Figure 4G**) or immunoblot (**Figure 4H**). Furthermore, while it did display a change in
254 electrophoretic mobility compatible with mitotic phosphorylation, unlike IRS2, it did not
255 decrease in abundance at mitotic exit in RPE1 cells (**Figure 4I**). Taken together, the
256 findings described above indicate that APC/C^{Cdh1} controls IRS2 levels in manner that is
257 dependent upon its C-terminal D-box motif.
258
259 *IRS2 is required for normal expression of many proteins involved in mitosis*
260 Many reported APC/C^{Cdh1} substrates (including several of those identified in our
261 initial proteomics screen) are required for normal cell cycle progression. Because
262 IR/IGF1R transduction promotes a variety of transcriptional programs (Copps and White,
263 2012), we hypothesized that IRS2 might promote the expression of proteins involved in
264 cell cycle control. To investigate this, we generated two IRS2 knockout RPE1 cell lines
265 using CRISPR/Cas9 (**Figure 5A)**, henceforth referred to as ΔIRS2-A and ΔIRS2-B. Using
266 these cells, we again employed TMT-coupled quantitative proteomics. The proteomes of
267 wild-type, ΔIRS2-A, and ΔIRS2-B cell lines were analyzed in biological triplicate, and
268 relative abundances were ascertained based on TMT reporter ion signal-to-noise values.
269 Hierarchical clustering indicated that the proteomes of the two knockout cell lines
270 analyzed were more similar to each other than either knockout cell line was to wild-type
271 (**Figure S5A**), indicating that deletion of IRS2 produced similar effects in both cell lines.
272 In order to exclude aberrancies that may have accrued during the CRISPR process or as
273 a result of clonal expansion, we focused the scope of our analysis to proteins that
274 changed significantly ($p < 0.05$) by more than 20% in both IRS2 knockout clones relative
275 to the WT cell line (**Figures 5B-5C**). We found 239 proteins that decreased by >20% in
276 both IRS2 knockout lines relative to the wild type line and 300 proteins that increased by
277 >20% (**Figures 5B-5C, S5B**).

278 We conducted gene enrichment analysis of the proteins that increased (**Figure**
279 **S5C**) or decreased (**Figure 5D**) by >20% in both knockout cell lines relative to wild type
280 cells. Of the 239 proteins that were depleted by >20% in both knockout cell lines, we
281 found a statistical over-representation of proteins participating in metabolic processes
282 characteristic of IR signal transduction. Notably, we also found an over-representation of
283 proteins involved in mitotic cell cycle regulation in this subset (**Figure 5D**). This suite of
284 proteins included regulators of mitotic entry and exit as well as several factors involved in
285 spindle assembly (**Figure 5E**). Consistent with the fact that strong depletion of most
286 critical cell cycle regulators renders cells inviable, most of the observed changes in cell
287 cycle-related genes were relatively modest (**Figure S5D**). Based on these data, we
288 conclude that IRS2 is important for promoting the expression of a suite of proteins
289 involved in orchestrating the mitotic cell cycle, and deletion of IRS2 stunts their expression
290 in RPE1 cells.
291
292 *IRS2 expression promotes a functional spindle assembly checkpoint*
293 Because many of the factors that were depleted in IRS2 knockout cell lines are
294 known to be involved in regulating spindle assembly and mitotic exit, we asked whether
295 IRS2 knockout cell lines display phenotypic differences from wild-type cells in terms of
296 spindle assembly checkpoint function. Using a high content nuclear imaging assay to
297 measure mitotic fraction based on DAPI staining intensity (Sackton et al., 2014), we asked
298 whether IRS2 knockout cell lines display mitotic arrest differences compared to wild-type
299 cells when treated with spindle poisons. Wild-type cells treated with nocodazole (a
300 microtubule destabilizing agent) arrested in mitosis in a dose-dependent manner,
301 whereas both IRS2 knockout cell lines displayed depressed mitotic arrest (**Figure 6A,**
302 **Figure S6A**). This was also true to a lesser extent in the presence of S-trityl-L-cysteine
303 (STLC), an Eg5 inhibitor (**Figure 6A**).
304 Using time lapse video microscopy, we found that untreated IRS2 knockout cell
305 lines had no significant alteration in mitotic duration compared to wild-type cells (**Figure**
306 **S6B**). In contrast, both IRS2 knockout cell lines had a significantly shorter mitotic duration
307 compared to wild-type cells ($p < 0.0001$ in both cases) when treated with 300 nM
308 nocodazole (**Figure 6B**). Importantly, wild-type cells expressing mAG1-geminin (1-101)—

309 an APC/C^{Cdc20} substrate that is stabilized by the spindle assembly checkpoint (Clijsters
310 et al., 2013)— display an accumulation of mAG1 fluorescence early in mitotic arrest,
311 consistent with checkpoint-mediated blockade of APC/C^{Cdc20}. In contrast, both IRS2
312 knockout cell lines display depressed mAG1 accumulation, consistent with higher
313 APC/C^{Cdc20} activity due to a weakened checkpoint (**Figure 6C**). This phenotype, along
314 with the shorter mitotic duration and lower mitotic fraction in the presence of spindle
315 poisons, is consistent with cells bearing a defective mitotic spindle assembly checkpoint.
316 Based on these data, we conclude that IRS2 promotes a functional spindle assembly
317 checkpoint in RPE1 cells.
318

319 **Discussion**

320 Based on the results of an unbiased proteomic screen, we provide evidence that
321 IRS2, a critical mediator of IR/IGF1R signaling, is a direct APC/C^{Cdh1} substrate. We
322 demonstrate that IRS2 is stabilized by APC/C inhibition and Cdh1 knockdown in multiple
323 cell types and that this depends on IRS2's C-terminal D-box motif. In contrast, we find
324 that IRS1, a closely related IRS2 paralog that lacks a D-box, is not subject to regulation
325 by the APC/C. Taken together, these results show that APC/C activity directly controls
326 IRS2 levels in a D-box dependent manner.

327 We identified a high-mobility form of IRS2 that accumulates under APC/C
328 inhibition, likely corresponding to a difference in phosphorylation given that IRS2 has
329 ~150 annotated threonine, serine, and tyrosine phosphorylation sites (Hornbeck et al.,
330 2015). This suggests that IRS2's APC/C-dependent stability could be regulated by
331 phosphorylation, possibly at sites near or within the D-box, which is an intriguing topic for
332 future study. Consistent with this, IRS2 phosphorylation is known to impact its stability in
333 other contexts, including following prolonged exposure to insulin or following mTOR
334 activation (Copps and White, 2012). Furthermore, there is a strong precedent for
335 phospho-regulation of APC/C degrons modulating substrate stability under specific
336 conditions (Holt, 2012; Mailand and Diffley, 2005; Wang et al., 2001).

337 Many APC/C substrates are involved in cell cycle regulation, and previous studies
338 have suggested a relationship between IRS2 and cell cycle progression. IRS2 can
339 stimulate cell cycle entry via Cdk4 activation (Chirivella et al., 2017) and is important for

340 sustaining proliferation in 32D myeloid cells and pancreatic β cells (Folli et al., 2011; Wu
341 et al., 2009). Based on these findings and our identification of IRS2 as an APC/C
342 substrate, we further investigated the role of IRS2 in regulating cell division. Proteomic
343 analyses of RPE1 cells lacking IRS2 reveal lower expression of well-characterized cell
344 cycle proteins compared to wild-type cells. Because these proteins are involved in critical
345 processes like cytokinesis, DNA replication, cell cycle transitions, and spindle assembly,
346 we investigated whether IRS2 knockout cell lines display cell cycle progression defects.
347 We find that cells lacking IRS2 have an impaired ability to arrest following spindle
348 assembly checkpoint activation in M-phase, thereby implicating IRS2 in promoting a
349 functional spindle assembly checkpoint.

350 Despite the well-established importance of sustained IRS2 levels in many tissue
351 types, little is known about what factors regulate its turnover. While several distinct
352 ubiquitin ligases control IRS1 stability (Fbxw8, Cbl-b, Fbxo40, SOCS1/3, MG53, and
353 others) (Nakao et al., 2009; Rui et al., 2002; Shi et al., 2011; Xu et al., 2008; Yi et al.,
354 2013), only SOCS1/3 have been implicated in the ubiquitin mediated proteolysis of IRS2
355 (Rui et al., 2002) until now. Thus, our work establishes APC/C^{Cdh1} as the first known
356 ubiquitin ligase that targets IRS2 but not IRS1. Furthermore, our results suggest that
357 APC/C^{Cdh1}-mediated IRS2 degradation is relevant in broad biological contexts since we
358 were able to demonstrate this mechanism of regulation in multiple cell lines.

359 Over the past several years, a number of connections between growth factor
360 signaling and APC/C-mediated regulation have emerged. SKIL/SnoN, an APC/C
361 substrate involved in TGFβ signaling, implicates APC/C activity in modulating the
362 expression of TGFβ target genes (Wan et al., 2001). Another APC/C substrate, CUEDC2,
363 controls the stability of the progesterone receptor (Zhang et al., 2007). Regarding
364 IR/IGF1R signaling, connections to APC/C-mediated regulation have been more opaque.
365 Multiple reports have shown that Cdh1 interacts with PTEN, a phosphatase that
366 antagonizes signal transduction through the IR pathway by dephosphorylating
367 phosphoinositide-3,4,5-triphosphate (PIP_3) (Choi et al., 2014; Song et al., 2011). Others
368 have demonstrated that components of the mitotic checkpoint complex (which inhibit
369 APC/C^{Cdc20}) potentiates IR signaling via IR endocytosis (Choi et al., 2019; Choi et al.,

370 2016). Despite these links, there have been no reports of direct APC/C substrates that
371 are involved in IR signaling until now.
372 Based on the data presented here, we propose a model (**Figure 7**) in which IRS2's
373 APC/C-mediated degradation in G_1 serves to limit IRS2-dependent signaling during G_1.
374 Upon APC/C inactivation at the G_1/S boundary, IRS2 is able to accumulate and stimulate
375 signaling required for normal progression through the latter stages of the cell cycle,
376 including the expression of proteins required for mitotic spindle checkpoint function. This
377 model is consistent with previous studies that implicate IRS2 in promoting the expression
378 of cell cycle-related genes, including mitotic cyclins (A and B) in mouse granulosa cells
379 (Lei et al., 2018). Furthermore, IR signal transduction promotes the expression of Plk1 (a
380 mitotic kinase) and CENP-A (a centromere protein) in β cells through a mechanism that
381 appears to depend on IRS2 rather than IRS1 (Folli et al., 2011; Shirakawa et al., 2017).
382 Our findings suggest that APC/C^{Cdh1} modulates IRS2-dependent signaling but not
383 IRS1-dependent pathways. In IRS2-deficient mice with consequent type 2 diabetes, some
384 have attributed the reduced β cell mass to a failure of β cells to re-enter the cell cycle
385 following division (Folli et al., 2011). Our findings that APC/C^{Cdh1} inhibition stabilizes IRS2
386 and that IRS2 promotes the expression of cell cycle regulatory proteins, coupled with data
387 from others showing that IRS2 can stimulate cell cycle entry (Chirivella et al., 2017),
388 suggest that APC/C^{Cdh1} inhibition may represent a possible approach for stimulating
389 proliferation in quiescent β cells via the stabilization of IRS2.
390

391 **Acknowledgements**

392 We thank the ICCB-Longwood Screening Facility at Harvard Medical School for
393 assistance with high content imaging assays and the Nikon Imaging Facility at Harvard
394 Medical School for assistance with time lapse and fluorescence microscopy. We thank
395 Kyle Copps, Pere Puigserver, and Christine Vogel for feedback on the manuscript. This
396 work was funded by NIH grant 1R35GM127032 to R.W.K.
397

398 **Author Contributions**

399 S.M. designed, performed, and analyzed all experiments aimed at identifying new APC/C
400 substrates in RPE1 cells. S.M. performed all experiments characterizing IRS2 as an

401 APC/C substrate. S.M. generated all recombinant cell lines used in this study and the
402 IRS2 CRISPR knockout cell lines. S.M. characterized mitotic arrest defects in IRS2
403 CRISPR knockout cell lines using time lapse microscopy and high-content imaging
404 assays. S.M. prepared all samples for mass spectrometry with assistance from Q.Y.
405
406 Q.Y. and S.P.G. performed mass spectrometry analysis of G_1 RPE1 cells treated with
407 APC/C inhibitors and IRS2 CRISPR knockout cell lines. Q.Y. and S.P.G. provided
408 reagents.
409
410 R.W.K. assisted with experimental design and data analysis.
411
412 S.M. and R.W.K. conceived of the project and wrote the manuscript with input from both
413 other authors.
414
415 **Declaration of Interests**
416 The authors declare no competing financial interests.
417
418 **Main Figure Legends**
419 ***Figure 1***: *High resolution chemical proteomics reveals proteins whose abundances are*
420 *APC/C regulated.*
421 (A) Workflow for the chemical proteomics experiment described in this study.
422 Asynchronous RPE1 cells were arrested in 1 μM palbociclib (a Cdk4/6 inhibitor) for
423 20 hours, at which point they were acutely treated with either DMSO or a combination
424 of 6 μM proTAME + 50 μM apcin (referred to as "APC/C inhibitors" or APCi). Cells
425 were then collected at time 0 (t_0, the time of drug addition) or 8 hours after drug
426 addition and were harvested for TMT-based proteomic identification and
427 quantification. Samples were analyzed in biological triplicate within a 10-plex TMT
428 label set, with the 10th channel used as a bridge.
429 (B) Asynchronous RPE1 cells were treated with either DMSO or 1 μM palbociclib for 20
430 hours. Cells were harvested, and lysates were analyzed by immunoblot for the
431 indicated proteins.

432 (C) Previously reported APC/C substrates that were identified in this study are plotted with
433 their observed fold change in the APC/C inhibitor treated sample (APCi) relative to
434 the DMSO treated sample. Error bars represent the standard deviation (SD) between
435 the three biological replicates measured by MS. Asterisks indicate an abundance
436 increase over control that is statistically significant (* : $p < 0.05$; ** : $p < 0.01$; *** : p
437 < 0.001 ; **** : $p < 0.0001$)
438 (D) Volcano plot highlighting all published APC/C substrates identified in this study (blue)
439 as well as proteins that (1) contain a high probability D- and/or KEN-box (D-box =
440 green, KEN-box = pink, D- and KEN-boxes = purple), (2) increase ≥1.147-fold under
441 APC inhibition, (3) were identified by >1 peptide, and (4) have a p-value < 0.05.
442
443 ***Figure 2***: *IRS2 levels are controlled by Cdh1 in a proteasome-dependent manner*
444 (A) Cells were treated identically to what is described in **Figure 1A**, and IRS2 abundance
445 was measured by immunoblot.
446 (B) C_2C_{12} myoblasts (Day 0) were induced to differentiate through serum withdrawal and
447 supplementation with insulin, transferrin, and selenium (ITS). After three days of
448 differentiation, myotubes were acutely treated with either DMSO or APC/C inhibitors
449 (of 6 μM proTAME + 50 μM apcin). After eight hours of drug treatment, myotubes were
450 collected and IRS2 levels from all samples were analyzed by immunoblotting.
451 (C)–(E) Asynchronous RPE1 (*C*), C_2C_{12} (*D*), and HeLa (*E*) cells were transfected with
452 either a control or Cdh1-directed siRNA for 24 hours. siRNAs were washed out of cell
453 culture media, and cells were allowed to grow for an additional 24 hours prior to
454 collection and analysis of IRS2 and Cdh1 levels in lysate by immunoblot.
455 (F) RPE1 cells were arrested in G_1 with 1 μM palbociclib for 20 hours. Following G_1
456 arrest, cells were treated with DMSO, APC/C inhibitors (6 μM proTAME + 50 μM
457 apcin), MG132 (10 μM), or a combination of APC/C inhibitors and MG132 for an
458 additional 8 hours. Cells were harvested, and lysates were analyzed by immunoblot
459 for IRS2 abundance.
460
461 ***Figure 3***: *IRS2 levels and phosphorylation fluctuate in a cell-cycle dependent manner*

462 (A) HeLa cells were synchronized by double thymidine block and released into S-phase.
463 Time points were taken every two hours for 14 hours. Lysates were harvested and
464 analyzed by immunoblotting for IRS2 and cell cycle markers (APC3 phosphorylation
465 and cyclin B1).
466 (B) HeLa cells were synchronized by thymidine-nocodazole block and released into
467 prometaphase. Mitotic cells were collected by mitotic shake-off and re-plated. Time
468 points were taken every two hours as cells exited M-phase. Lysates were harvested
469 and analyzed by immunoblotting for IRS2 and cell cycle markers (APC3
470 phosphorylation and cyclin B1).
471 (C) RPE1 cells were synchronized in prometaphase by 7.5 μM RO3306 treatment. After
472 18 hours, cells were switched to fresh media and were allowed to enter mitosis (~35
473 minutes following drug removal). At mitotic entry, cells were collected by mitotic shake-
474 off and were re-plated (0 hr). Time points were taken as cells exited M-phase and
475 entered G_1. Lysates were harvested and analyzed by immunoblotting for IRS2 and
476 cell cycle markers (APC3 phosphorylation and cyclin B1).
477
478 ***Figure 4***: *Cdh1's ability to control IRS2 levels depends on a C-terminal D-box motif*
479 (A) (*top*) Schematic depicting IRS2's protein domain structure. PH = pleckstrin homology
480 domain, PTB = phosphotyrosine binding domain, KRLB = kinase regulatory-loop
481 binding region. IRS2's C-terminal full D-box motif is highlighted in red. (*bottom*)
482 Comparison of IRS2's D-box conservation among placental mammals.
483 (B) RPE1 cells stably expressing lentivirus-derived, doxycycline-inducible, C-terminally
484 HA-tagged IRS2 constructs were arrested in G_1 with 1 μM palbociclib for 20 hours.
485 Following arrest, samples were either collected or DMSO or APC inhibitors (6 μM
486 proTAME + 50 μM apcin) were added for an additional 8 hours. Quantification of
487 immunoblots shown at right: HA levels were normalized to a loading control and are
488 plotted relative to DMSO levels. Error bars = mean ± SEM. * : p=0.0187; ns : p=0.816
489 (C) C_2C_{12} myoblasts stably expressing lentivirus-derived, doxycycline-inducible, C-
490 terminally HA-tagged IRS2 constructs were grown to confluence and switched to low
491 serum media supplemented with ITS (differentiation media, DM) and doxycycline.
492 Cells were allowed to differentiate into myotubes for three days (with media

493 refreshment every 24 hours), at which point (0 hr) either DMSO or APC/C inhibitors (6
494 μM proTAME + 50 μM apcin) for an additional 8 hours in the presence of doxycycline.
495 Quantification of immunoblots shown at right: HA levels were normalized to a loading
496 control and are plotted relative to DMSO levels. Error bars = mean ± SEM. * :
497 p=0.0118; ns : p=0.910.
498 (D) Asynchronous RPE1 cells stably expressing lentivirus-derived, doxycycline-inducible
499 C-terminally HA-tagged IRS2 constructs were transfected with a non-targeting
500 (control) siRNA or an siRNA directed against Cdh1 for 24 hours. Quantification of
501 immunoblots shown at right: HA levels were normalized to a loading control and are
502 plotted relative to DMSO levels. Error bars = mean ± SEM. * : p=0.0132; ns : p=0.963.
503 (E) Asynchronous HeLa cells stably expressing lentivirus-derived, N-terminally FLAG-HA
504 tagged IRS2 constructs were transfected with a non-targeting (control) siRNA or an
505 siRNA directed against Cdh1 for 24 hours. Quantification of immunoblots shown at
506 right: HA levels were normalized to a loading control and are plotted relative to DMSO
507 levels. Error bars = mean ± SEM. * : p=0.0131; ns : p=0.803.
508 (F) Comparison of the Hs IRS2 D-box sequence with the aligned area on Hs IRS1.
509 (G) MS-quantified IRS1 and IRS2 abundance in G_1 APC inhibitor proteomics. IRS1
510 abundance was quantified based on 5 peptides (4 unique) in 3 biological replicates;
511 IRS2 was quantified based on 3 peptides (all unique) in 3 biological replicates.
512 (H) RPE1 cells were subject to the same conditions described in Figure 1A, and cell
513 lysates were analyzed by immunoblotting for IRS1 abundance
514 (I) RPE1 cells were synchronized in late G_2 with 7.5 μM RO3306 for 18 hours. Cells
515 were released into fresh media and allowed to enter mitosis (~35 min post-drug
516 removal) and were collected by mitotic shake-off. Mitotic cells were re-plated and
517 collected at the indicated time points. Cell lysates were analyzed by immunoblotting
518 for IRS1 abundance.
519
520 ***Figure 5***: *IRS2 knockout cell lines are defective in mitotic cell cycle-related protein*
521 *expression*.
522 (A) WT, ΔIRS2-1, and ΔIRS2-2 cell line lysates were analyzed for IRS2 expression by
523 immunoblotting.

524 (B-C) Volcano plots comparing proteomes of ΔIRS2 cell lines with WT cell line. Proteins
525 that significantly decrease > 20% (p-value<0.05) in both cell lines compared to wild-
526 type are shown in purple; proteins that significantly increase > 20% (p-value<0.05) in
527 both cell lines compared to WT are shown in green.
528 (D) Gene ontology (GO) term enrichment of proteins that decrease in both ΔIRS2 cell lines
529 relative to WT cells.
530 (E) Heat map depicting cell cycle-related protein abundance changes between ΔIRS2 cell
531 lines and WT cells.
532
533 ***Figure 6***: *IRS2 expression promotes a functional spindle assembly checkpoint.*
534 (A) Mitotic fractional analysis for RPE1 wild type (WT) and IRS2 KO cell lines treated with
535 the indicated doses of nocodazole and S-trityl L-cysteine (STLC) for 18 hours. Mitotic
536 fraction measurements were made using a high content fixed cell imaging assay
537 based on DAPI intensity of stained nuclei. Error bars = mean ± SD.
538 (B) Asynchronous RPE1 wild type (WT) or IRS2 KO cell lines were treated with 300 nM
539 nocodazole and imaged every five minutes by widefield time lapse microscopy for 36
540 hours. Each point represents an individual cell's mitotic duration, measured as the
541 time from nuclear envelope breakdown (NEB) to division, slippage, or cell death. Error
542 bars = mean± SD. *p*-values were calculated by one-way ANOVA. **** = $p<0.0001$. ns
543 = not statistically significant.
544 (C) Asynchronous RPE1 wild type (WT) or IRS2 KO cell lines expressing mAG1-
545 geminin(1-110) were treated as in (C). mAG1 fluorescence intensity was measured
546 from nuclear envelope breakdown (NEB) until division, slippage, or cell death (n=10
547 for all three cell lines). Error bars = mean ± SEM. Fluorescence intensity was
548 background subtracted and normalized to intensity at NEB.
549
550 ***Figure 7***: Model for IRS2's role in cell cycle control. IRS2 is targeted for proteasomal
551 degradation by APC/C^{Cdh1} during G_1. When APC/C is inactivated at the G_1/S boundary,
552 IRS2 protein accumulates, potentially allowing it to stimulate the expression of cell cycle-
553 related proteins either through IR-mediated action (Shirakawa et al., 2017) or through
554 another receptor tyrosine kinase. Some of the proteins that are expressed through this

555 pathway may be required for a robust spindle assembly checkpoint, which directly inhibits
556 APC/C^{Cdc20} during M-phase.
557
558 **Tables**
559 ***Table 1***: 26 proteins containing high-probability D- and KEN-boxes as identified from G_1
560 APC/C inhibitor proteomics.

Gene Symbol	Fold Change	KEN box	D box	Similarity score(s) [a]	Consensus similarity [b]	Disorder Score [c]	Citation [d]
TK1	3.6	Y		0.97	High	0.53	(Ke et al., 2005)
CKAP2	3.2	Y	Y	0.95 ; 0.81	High ; Medium	0.62 ; 0.49	(Seki and Fang, 2007)
KIF11	2.4	Y	Y	0.97 ; 0.84	High ; High	0.57 ; 0.52	(Eguren et al., 2014)
GMNN [e]	2.2	Y	Y	0.80 ; 0.81	Low ; Medium	0.61 ; 0.66	(McGarry and Kirschner, 1998)
TACC3	1.9	Y (2)		0.94/0.90	High/High	0.54/0.49	(Jeng et al., 2009)
TOP2A	1.8	Y		0.86	High	0.44	(Eguren et al., 2014)
MKI67	1.5	Y (2)		0.89/0.86	High/High	0.45/0.48	
CUEDC2	1.4	Y		0.99	High	0.71	(Zhang et al., 2013)
IRS2	1.3		Y	0.87	High	0.68	
GPBP1	1.3	Y		0.81	Medium	0.61	
BUB1B	1.2	Y (2)	Y (2)	0.92/0.85 ; 0.83/0.86	High/Medium ; High/High	0.47/0.64 ; 0.47/0.49	(Choi et al., 2009)
UHRF2	1.2	Y		0.88	High	0.61	
PBXIP1	1.2		Y	0.83	Medium	0.42	(Khumukcham et al., 2019)
DCBLD1	1.2		Y	0.86	High	0.56	
KIF23	1.2	Y		0.87	High	0.45	(Singh et al., 2014)
ULK1	1.2		Y	0.85	High	0.58	
NAA38	1.2		Y	0.82	Medium	0.44	
LRP10	1.2		Y	0.82	Medium	0.49	
PNPLA8	1.2	Y		0.92	High	0.61	
CEP120	1.2		Y	0.84	High	0.42	
DIAPH3 [f]	1.2		Y	0.84	High	0.56	(DeWard and Alberts, 2009)
KDM2A	1.2	Y		0.94	High	0.66	
PRPF38B	1.2	Y		0.92	High	0.44	
DLGAP5	1.2	Y		0.89	High	0.6	(Song and Rape, 2010)
KDM3A	1.2	Y	Y	0.95 ; 0.81	High ; Medium	0.59 ; 0.48	
ANKRD11	1.2		Y	0.86	High	0.53	

561 Features of the putative degron(s) found in each protein are annotated, including (a) the
562 SLiMSearch similarity score to other validated degrons, (b) the similarity of the
563 surrounding consensus sequence to other validated degrons, (c) the disorder score for
564 the region of the protein in which the degron is located, and (d) the citation of the
565 publication that reports the protein as an APC/C substrate, where applicable. (e) We
566 cannot delineate whether the geminin peptides identified here derive from the FUCCI
567 reporter or the endogenous protein. (f) While DIAPH3/mDia2 has been shown to be
568 ubiquitinated in a cell cycle dependent manner and was suggested as an APC/C
569 substrate, there is no direct cell-based or biochemical evidence for this. Previously
570 reported substrates are shown in bold.
571
572 **STAR Methods**
573 ***Cell Culture and Synchronization***
574 All cell lines used in this work (HeLa, C_2C_{12}, hTERT-RPE1-FUCCI, HEK293T) were
575 cultured in a humidified incubator at 37ºC in the presence of 5% CO_2. HeLa, hTERT-
576 RPE1 and C_2C_{12} cells were obtained from American Type Culture Collection (ATCC), and
577 hTERT-RPE1 cells were modified with FUCCI constructs(Sakaue-Sawano et al., 2008)
578 with the permission of the RIKEN Institute. HeLa cells were grown in DMEM with 10%
579 FBS. Proliferating C_2C_{12} myoblasts were grown in DMEM with 15% FBS, whereas
580 differentiated myotubes were cultured in differentiation media, consisting of DMEM with
581 2% horse serum and 1x insulin, transferrin, selenium (ITS) Premix Universal Culture
582 Supplement (Corning, 354350). hTERT-RPE1-FUCCI cells were grown in DMEM/F12
583 with 10% FBS supplemented with 0.01 mg/ml hygromycin B (Corning, 30-240-CR).
584 HEK293T cells used for lentivirus generation were a gift from Wade Harper and were
585 cultured in DMEM with 10% FBS. All cell lines tested were negative for mycoplasma
586 contamination (Lonza LT07-218).
587
588 HeLa cells were synchronized by double thymidine block by treating with 2 mM thymidine
589 for 18 hours, releasing for 8 hours, and re-treating with 2 mM thymidine for 19 hours.
590 HeLa cells synchronized by thymidine-nocodazole block were treated with 2 mM
591 thymidine for 20 hours, released for 8 hours, then treated with 300-330 nM nocodazole

592 for 15 hours. Mitotic cells were collected by shake-off and re-plated in drug-free media for
593 cell cycle time course experiments.
594
595 RPE1 cells were synchronized by RO3306 treatment by treating with 7.5 μM RO3306 for
596 18 hours before releasing into fresh media for 30-40 minutes, after which cells were
597 collected by mitotic shake-off and re-plated for cell cycle time course experiments. For G_1
598 arrest experiments, RPE1 cells were treated with 1 μM palbociclib for 20 hours.
599
600 To differentiate C_2C_{12} myoblasts into myotubes, cells were grown to confluence and
601 washed 2x in DMEM with 2% horse serum before switching to differentiation media. Cells
602 were incubated for 72 hours, with media changes every 24-36 hours. Differentiation into
603 myotubes was confirmed visually as well as by immunoblotting for MyoD, a myogenic
604 marker.
605
606 ***Immunoblotting***
607 Cell extracts were prepared in lysis buffer (10 mM Tris HCl pH 7.4, 100 mM NaCl, 1 mM
608 EDTA, 1 mM EGTA, 1 mM NaF, 1 mM PMSF, 20 mM $Na_4P_2O_7$, 2 mM NA_3VO_4, 1% Triton
609 X-100, 10% glycerol, 0.1% SDS, and 0.5% deoxycholate) supplemented with Pierce
610 protease inhibitor tablets (Thermo Fisher Scientific, A32963) and Pierce phosphatase
611 inhibitor tablets (Thermo Fisher Scientific, A32957). Pellets were incubated in lysis buffer
612 on ice for 30 minutes with vortexing and were centrifuged at 13,000rpm for 10 minutes to
613 clear the lysate. Protein concentrations were determined using a bicinchoninic acid (BCA)
614 assay (Thermo Fisher Scientific, 23225). Supernatants were re-suspended in NuPAGE
615 LDS sample buffer (Thermo Fisher Scientific, NP0008) supplemented with 100 mM
616 dithiothreitol (DTT) and boiled at 100ºC for 5 minutes. Equal masses of lysates were
617 separated by SDS-PAGE using either 4-12% Bis Tris gels or 3-8% Tris acetate gels
618 (Thermo Fisher Scientific). All IRS2 immunoblots were separated on 3-8% Tris acetate
619 gels with the exception of those shown in **Figures 5A** and **S4B**, which were separated on
620 4-12% Bis Tris gels. Proteins were transferred to polyvinylidene difluoride (PVDF)
621 membranes (Thermo Fisher Scientific, 88518).
622

623 Membranes were blocked in 5% non-fat dry milk in Tris-buffered saline with 0.1% Tween
624 (TBS-T) before incubating with primary antibodies overnight at 4ºC with agitation.
625 Membranes were probed with secondary antibodies dissolved in 5% milk in TBS-T for 1-
626 2 hours at room temperature before developing with an Amersham 600RGB imaging
627 system. Quantification of immunoblots was done using ImageJ (Schneider et al., 2012).
628
629 ***Antibodies***
630 The following commercially available primary antibodies were used for immunoblotting:
631 anti-IRS2 (Cell Signaling Technologies, 4502) 1:750; anti-Cdh1/Fzr1 (Sigma Aldrich,
632 CC43) 1:500; anti-APC3 (BD Transduction Laboratories, 610455) 1:500; anti-cyclin B1
633 (Santa Cruz Biotechnology, sc-752) 1:500; anti-Cdc20 (Santa Cruz Biotechnology, sc-
634 8358) 1:500; anti-HA-peroxidase (Sigma Aldrich), 1:1500; anti-cyclin A2 (Santa Cruz
635 Biotechnology, sc-596) 1:500; anti-IRS1 (Cell Signaling Technologies, 2382) 1:750; anti-
636 MyoD1 (Cell Signaling Technologies, 13812) 1:750; anti-GAPDH (Abcam, ab8245)
637 1:2000; anti-α tubulin (Abcam, ab7291 and Santa Cruz Biotechnology, sc-8035) 1:1000
638 for both; anti-vinculin (Santa Cruz Biotechnology, sc-73614) 1:2000. Secondary
639 antibodies used: anti-rabbit IgG-HRP (GE Healthcare, NA934) and anti-mouse IgG- HRP
640 (GE Healthcare, NA931V), both at 1:3000 dilutions.
641
642 ***Compounds***
643 The following chemicals were used: palbociclib (LC Laboratories, P-7722), proTAME
644 (Boston Biochem, I-440), MG132 (474790, Calbiochem), S-trityl L-cysteine (STLC, Alfa
645 Aesar, L14384), thymidine (Sigma Aldrich, T9250), nocodazole (Sigma Aldrich, 31430-
646 18-9), RO3306 (AdipoGen Life Sciences, AGCR13515M), doxycycline hyclate (Sigma
647 Aldrich, D9891). Apcin was custom synthesized by Sundia MediTech Company (Lot
648 #A0218-10069-031) using methods described previously (Sackton et al., 2014). All
649 compounds were dissolved in dimethyl sulfoxide (DMSO), with the exception of thymidine
650 and doxycycline, which were dissolved in Dulbecco's phosphate buffered saline (DPBS,
651 Corning, 21-030-CV). Dissolved compounds were stored at -20°C prior to use.
652
653 ***CRISPR/Cas9 mediated gene editing***

654 A TrueGuide crRNA directed against exon 1 of Hs IRS2's coding region (target DNA
655 sequence: 5'- TCG AGA GCG ATC ACC CGT TT -3', Assay ID number:
656 CRISPR850215_CR, Thermo Fisher Scientific) was annealed to the TrueGuide tracrRNA
657 (Thermo Fisher Scientific, A35507) according to manufacturer protocol. hTERT RPE1-
658 FUCCI cells were co-transfected with TrueCut Cas9 protein v2 (Thermo Fisher Scientific,
659 A36496) and the annealed tracrRNA:crRNA complex using the Lipofectamine
660 CRISPRMAX Cas9 Transfection reagent (Thermo Fisher Scientific, CMAX00003)
661 according to manufacturer protocol. Transfected cells were incubated for two days before
662 switching to fresh media and expanding. Single cell clones were isolated using the limiting
663 dilution method in a 96-well format, and clonal cell lines were expanded before screening
664 for knockouts by immunoblotting.
665
666 ***Site directed mutagenesis***
667 R777-E111 Hs.IRS2 and R777-E111 Hs.IRS2-nostop were gifts from Dominic Espositio
668 (Addgene plasmid #70395 and #70396, respectively). Both of these plasmids encode
669 codon optimized sequences for IRS2, with and without a stop codon respectively. R972A
670 mutations were introduced into the aforementioned IRS2 clones using the Q5 Site-
671 Directed Mutagenesis Kit (New England BioLabs) with the primers 5' - AGA TTA TAT
672 GAA TAA GTC CAC TGT CAG ATT ATA TG - 3' and 5' - GAC AGT GGA CTT GCC TGG
673 CGA GAG TCT GAA CT - 3' according to the manufacturer's protocol. For N-terminally
674 FLAG-HA-tagged constructs, the insert from R77-E111 Hs.IRS2 (WT or ∆D) was cloned
675 into the pHAGE-FLAG-HA-NTAP vector (a gift from Wade Harper) using the Gateway LR
676 Clonase II system (Invitrogen). For doxycycline-inducible, C-terminally HA-tagged
677 constructs, the insert from R77-E111 Hs.IRS2-nostop (WT or ∆D) was cloned into
678 pINDUCER20 (a gift from Stephen Elledge, Addgene plasmid #44012) using the Gateway
679 LR Clonase II system (Invitrogen). The ∆D mutation was verified both before and after
680 Gateway cloning by Sanger sequencing.
681
682 ***Lentivirus construction***
683 To construct lentiviruses, HEK293T cells were co-transfected with pPAX2, pMD2, and
684 either pINDUCER-20-IRS2 or pHAGE-FLAG-HA-NTAP-IRS2 in a 4:2:1 DNA ratio using

685 Lipofectamine 3000 (Invitrogen, L3000001) according to manufacturer's instructions.
686 pPAX2 and pMD2 were gifts from Wade Harper. 24 hours after transfection, HEK293T
687 cells were switched to fresh media (DMEM + 10% FBS). 48 hours after transfection
688 lentiviruses were harvested by clearing debris by centrifugation at 960*xg* for 5 minutes
689 and filtering through 0.45 µm SFCA filters. Lentiviruses were either used immediately or
690 flash frozen in liquid nitrogen and stored at -80ºC for later use.
691
692 ***Stable cell line construction***
693 To generate stable cell lines, plated HeLa, RPE1, or C_2C_{12} cells were incubated with
694 lentiviruses and 2 µg/ml protamine sulfate. 24 hours after viral infection, cells were
695 switched to fresh media. 48 hours after viral infection, antibiotics were introduced. For
696 lentiviruses derived from pINDUCER20, geneticin (Invitrogen, 10131027) was used at a
697 concentration of 750 µg/ml for both RPE1 and C_2C_{12} for 6-7 days. For lentiviruses derived
698 from pHAGE-FLAG-HA-NTAP, puromycin (Sigma Aldrich, P8833) was used at a
699 concentration of 0.5 µg/ml for 3 days. Antibiotic-selected populations of cells were
700 expanded and used for further experiments without clonal selection.
701
702 ***Small interfering RNAs (siRNAs)***
703 Cells were transfected using RNAiMax (Invitrogen, 13778100) according to
704 manufacturer's instructions with the following siRNAs: siGENOME Non-Targeting Control
705 siRNA #5 (D-001210-05, Dharmacon); ON-TARGETplus Human FZR1 siRNA (J-015377-
706 08, Dharmacon), 25 nM; SMARTpool ON-TARGETplus Mouse Fzr1 siRNA (L-065289-
707 01-0005), 25 nM. Cells were treated with siRNAs for 24 hours for all experiments. For
708 experiments involving subsequent compound treatment, cells were switched to fresh
709 media prior to the addition of compounds.
710
711 ***Plasmid transfection***
712 C_2C_{12} myoblasts were transfected with a plasmid containing the N-terminal 88 amino
713 acids of human cyclin B1 fused to EGFP using Lipofectamine 3000 (Invitrogen,
714 L3000001) with the P3000 reagent according to manufacturer's instructions. Growth

715 media was refreshed to remove transfection reagents 24 hours post-transfection, and
716 cells were switched to differentiation media for an additional 3 days.
717
718 ***Time lapse and fluorescence microscopy***
719 Cells were plated in a 24-well coverslip-bottom plate (Greiner BioOne, 662892). After 24
720 hours, cells were treated with the indicated compounds and were imaged immediately
721 afterwards. Plates were inserted into a covered cage microscope incubator (OkoLab) with
722 temperature and humidity control at 37ºC and 5% CO_2 and mounted on a motorized
723 microscope stage (Prior ProScan III). All images were collected on a Nikon Ti motorized
724 inverted microscope equipped with a 20x/0.75 NA Plan Apo objective lens and the Perfect
725 Focus system. mCherry fluorescence was excited with a Lumencor Spectra-X using a
726 555/25 excitation filter and a 605/52 emission filter (Chroma). mAG1 fluorescence was
727 excited using a 490/20 excitation filter and a 525/36 emission filter (Chroma). Both
728 configurations used a Sedat Quad dichroic (Chroma). Images were acquired with a
729 Hamamatsu Orca-R2 or Hamamatsu Flash 4.0 V2 controlled with Nikon Elements image
730 acquisition software. Three fields of view were collected per condition, and phase contrast
731 and/or fluorescence images were captured at 5- to 8-minute intervals (depending upon
732 the experiment) for 24-48 hours.
733
734 Videos were analyzed using ImageJ. Mitotic duration was defined as the time from
735 nuclear envelope breakdown (NEB) until division, death (cytoplasmic blebbing), or mitotic
736 slippage. mAG1 and mCherry intensities were quantified manually by measuring the
737 maximum intensity of signal for each cell in a given frame across multiple time points. For
738 experiments analyzing fluorescence intensity during G_1 arrest, measurements were made
739 for all cells in a frame for each time point.
740
741 ***TMT mass spectrometry sample preparation***
742 Cells were cultured as described in biological triplicate. Cells pellets were re-suspended
743 in urea lysis buffer: 8M urea, 200 mM EPPS pH 8.0, Pierce protease inhibitor tablets
744 (Thermo Fisher Scientific, A32963), and Pierce phosphatase inhibitor tablets (Thermo
745 Fisher Scientific, A32957). Lysates were passed through a 21-gauge needle 20 times,

746 and protein concentrations were measured by BCA assay (Thermo Fisher Scientific). 100
747 µg of protein were reduced with 5 mM tris-2-carboxyethyl-phosphine (TCEP) at room
748 temperature for 15 minutes, alkylated with 10 mM iodoacetamide at room temperature for
749 30 minutes in the dark, and were further reduced with 15 mM DTT for 15 minutes at room
750 temperature. Proteins were precipitated using a methanol/chloroform extraction. Pelleted
751 proteins were resuspended in 100 µL 200 mM EPPS, pH 8.0. LysC (Wako, 125-05061)
752 was added at a 1:50 enzyme:protein ratio, and samples were incubated overnight at room
753 temperature with agitation. Following overnight incubation, trypsin (Promega, V5111) was
754 added at a 1:100 enzyme:protein ratio, and samples were incubated for an additional 6
755 hours at 37ºC. Tryptic digestion was halted by the addition of acetonitrile (ACN). Tandem
756 mass tag (TMT) isobaric reagents (Thermo Fisher Scientific, 90406) were dissolved in
757 anhydrous ACN to a final concentration of 20 mg/mL, of which a unique TMT label was
758 added at a 2:1 label:peptide ratio. Peptides were incubated at room temperature for one
759 hour with vortexing after 30 minutes. TMT labeling reactions were quenched by the
760 addition of 10 µL of 5% hydroxylamine. Equal amounts of each sample were combined
761 at a 1:1 ratio across all channels and lyophilized by vacuum centrifugation. Samples were
762 re-suspended in 1% formic acid (FA)/99% water and were desalted using a 50 mg 1cc
763 SepPak C18 cartridge (Waters, WAT054955) under vacuum. Peptides were eluted with
764 70% ACN/1% FA and lyophilized to dryness by vacuum centrifugation. The combined
765 peptides were fractionated with basic pH reversed-phase (BPRP) HPLC, collected in a
766 96-well format and consolidated to a final of 24 fractions, out of which only alternating
767 fractions (a total of 12) were analyzed (Navarrete-Perea et al., 2018). Each fraction was
768 desalted via StageTip, lyophilized to dryness by vacuum centrifugation, and reconstituted
769 in 5% ACN/5% FA for LC-MS/MS processing.
770
771 ***TMT mass spectrometry analysis***
772 Data for the G_1 APC inhibition experiment were collected on an Orbitrap Fusion mass
773 spectrometer coupled to a Proxeon EASY-nLC 1000 liquid chromatography (LC) pump
774 (Thermo Fisher Scientific), whereas data for IRS2 knockout cell line analysis were
775 collected on an Orbitrap Fusion Lumos mass spectrometer coupled to a Proxeon EASY-
776 nLC 1200 liquid chromatography (LC) pump. The 100 µm capillary column was packed

777 with 30 cm of Accucore 150 resin (2.6 µm, 150Å; Thermo Fisher Scientific). Mobile
778 phases were 5% ACN, 0.125% FA (Buffer A) and 95% ACN, 0.125% FA (Buffer B).
779 Peptides from G_1 APC inhibition experiment were separated using a 2.5 h gradient from
780 4% to 26% Buffer B and analyzed with a SPS-MS3 method (McAlister et al., 2014).
781 Peptides from IRS2 knockout cell line analysis were separated using a 2 h gradient from
782 4% to 30% Buffer B and analyzed with a real-time search strategy (Erickson et al., 2019;
783 Schweppe et al., 2019).
784
785 Raw data were converted to mzXML format using a modified version of RawFileReader
786 and searched against a human protein target-decoy database. Searches were performed
787 with a 50 ppm precursor mass tolerance, 0.9 Da fragment mass tolerance, trypsin digest
788 with up to 2 missed cleavages. Allowed modifications include cysteine
789 carboxyamidomethylation (+57.02146), static TMT on lysine and peptide N-temini
790 (+229.16293) and up to 3 variable methionine oxidation (+15.99491). Peptide spectral
791 matches were filtered with a linear discriminant analysis (LDA) method to a 1% FDR
792 (Huttlin et al., 2010) and a protein-level FDR of 1% was also implemented (Savitski et al.,
793 2015). For peptide quantification, we extracted the TMT signal-to-noise and column
794 normalized each channel to correct for equal protein loading. Peptide spectral matches
795 with summed signal-to-noise less than 100 were excluded from final result. Lastly, each
796 protein was scaled such that the summed signal-to-noise for that protein across all
797 channels equals 100, thereby generating a relative abundance (RA) measurement.
798
799 ***High content mitotic fraction assay***
800 Asynchronous hTERT RPE1-FUCCI wild-type or IRS2 KO cell lines were plated in a
801 black, clear-bottom 96-well plate (Corning, 3606). Plates were sealed with breathable
802 white rayon sealing tape (Nunc, 241205) to prevent evaporation following plating and
803 during all subsequent incubations. In experiments involving RNAi, cells were treated with
804 siRNAs for 24 hours. Cells were switched to fresh media, and compounds were added at
805 the indicated concentrations for an additional 18 hours. Following compound treatment,
806 cells were fixed and stained directly without additional washing steps (to avoid the loss of
807 loosely attached mitotic cells) with 10% formalin, 0.33 µg/mL Hoechst 33342, and 0.1%

808 Triton X-100 in DPBS. Plates were sealed with aluminum tape (Nunc, 276014) and were
809 incubated for 45 minutes room temperature in the dark before imaging. All experimental
810 conditions were represented in triplicate on the same plate. Plates were imaged using an
811 ImageXpress Micro high-content microscope (Molecular Devices) equipped with a 10x
812 objective lens. Four images were acquired per well, yielding a total of 12 images per
813 conditions. Images were processed automatically in ImageJ to identify and count nuclei
814 as well as measure their maximum fluorescence intensity. ImageJ output files were
815 pooled, and cumulative frequency curves for the maximum intensity of the cell population
816 in each condition were computed using MATLAB. An intensity threshold was set based
817 on the intensity of mitotic cells in control (DMSO-treated) wells to delineate interphase
818 cells from mitotic cells. The fraction of mitotic cells was calculated as the fraction of cells
819 above the set intensity threshold in MATLAB(Sackton et al., 2014).
820
821 ***Statistical analyses***
822 For experiments regarding the stability of IRS2-WT and IRS2-ΔD, *p*-values were
823 calculated by two-way ANOVA. For fluorescence microscopy experiments that quantify
824 mAG1 intensity in response to drug treatment over time, *p*-values were calculated by two-
825 way ANOVA. For microscopy experiments that quantify mitotic duration following
826 nocodazole treatment, *p*-values were calculated by one-way ANOVA. For proteomics
827 data, *p*-values were calculated using a two-tailed, unpaired Student's t-test. For time
828 lapse microscopy data, *p*-values were calculated by one-way ANOVA. Gene enrichment
829 was calculated using the AmiGO 2 search tool (Carbon et al., 2009). Error bars indicate
830 standard deviation (SD) or standard error of the mean (SEM) where indicated.
831
832 ***Materials Availability***
833 All mass spectrometry raw files will be available through the PRIDE archive upon
834 publication. All other data are available in the associated supplementary data files.
835 Further information and requests for resources and reagents should be directed to the
836 Lead Contact, Randy King (randy_king@hms.harvard.edu).
837
838 **Supplemental Information Legends**

839 ***Figure S1***: *Related to Figure 1*

840 (A) Asynchronous RPE1 cells were treated with 1 μM palbociclib and imaged by
841 fluorescence time lapse microscopy for 20 hours. Frames at 0, 10, and 20 hours are
842 shown.

843 (B) From the experiment shown in Figure S1B, FITC intensity was quantified at 0 hours
844 (time of drug addition) and 20 hours. Each point represents the maximum FITC
845 intensity of an individual cell at the given time point. ns : not significant ; **** :
846 $p<0.0001$.

847 (C) Asynchronous RPE1 cells were treated with 1 μM palbociclib for 20 hours. Following
848 G_1 arrest, cells were treated with either DMSO or APC inhibitors (6 μM proTAME + 50
849 μM apcin) and imaged by fluorescence widefield time lapse microscopy for an
850 additional eight hours.

851 (D) Quantification of the experiment shown in S1D, as explained in S1B. Error bars = SD
852 among all of the cells quantified for each condition. ns: not significant ; **** : $p<0.0001$.

853

854 ***Figure S2***: *Related to Figure 2B*

855 (A) Asynchronous C_2C_{12} myoblasts and 3-day differentiated C_2C_{12} myotubes were lysed
856 and MyoD levels were measured by immunoblotting.

857 (B) Phase-contrast images of asynchronous (Day 0) C_2C_{12} myoblasts and 3-day
858 differentiated C_2C_{12} myotubes.

859 (C) Asynchronous C_2C_{12} myoblasts were transfected with a plasmid coding for the N-
860 terminal fragment of cyclin B1 (amino acids 1-88) fused to EGFP for 24 hours.
861 Following transfection, cells were switched to low-serum differentiation media
862 containing ITS for three days with media refreshment every 24 hours. After 3 days,
863 myotubes were acutely treated with either DMSO or APC inhibitors (6 μM proTAME +
864 50 μM apcin) for an additional 8 hours. Myotubes were then harvested, and lysates
865 were analyzed for transgene expression by immunoblot.

866

867 ***Figure S3***: *Related to Figure 3*

868 (D) HeLa cells were synchronized by double thymidine block and released into S-phase
869 either in the presence of DMSO or 5 μM RO3306. Cells were harvested at the

870 indicated time points for analysis of the given protein abundances and phosphorylation
871 patterns in lysate by immunoblot.
872
873 ***Figure S4***: *Related to Figure 4*
874 (A) *(left)* RPE1 cells stably expressing lentivirus generated, C-terminally HA-tagged IRS2
875 wild type (WT) and R972A (ΔD) constructs were arrested in G_1 with 1 μM palbociclib
876 for 20 hours. Cells were then acutely treated with either DMSO or the indicated dose
877 range of APC inhibitors for an additional 8 hours. Cells were then harvested, and
878 lysate was analyzed for HA expression by immunoblot. The lane denoted t_0 indicates
879 a sample that was collected at the time of drug addition. (*right*) The experiment shown
880 at left was repeated three times, and HA intensity was quantified. Plot shows HA
881 intensity normalized to a loading control (either GAPDH or Ponceau) and to the DMSO
882 condition. Error bars = mean ± SEM.
883 (B) (*top*) Asynchronous RPE1 cells expressing doxycycline-inducible, C-terminally HA
884 tagged IRS2 variants were treated with a dose range of doxycycline. HA and IRS2
885 expression levels were analyzed by immunoblotting cell lysates. Red = doxycycline
886 dose used for all experiments. (*bottom*) Asynchronous C_2C_{12} cells expressing
887 doxycycline-inducible, C-terminally HA tagged IRS2 variants were treated with a dose
888 range of doxycycline. HA and IRS2 expression levels were analyzed by
889 immunoblotting cell lysates. Red = doxycycline dose used for all experiments.
890
891 ***Figure S5***: *Related to Figure 5*
892 (A) Hierarchical clustering for the nine conditions analyzed by TMT-coupled quantitative
893 mass spectrometry in wild type and ΔIRS2 cell lines.
894 (B) Venn diagrams depicting proteins that (*left*) decrease significantly >20% relative to
895 WT cells in both ΔIRS2 cell lines and (*right*) increase significantly >20% relative to WT
896 in both ΔIRS2 cell lines.
897 (C) Gene ontology (GO) term enrichment of proteins that increase in both ΔIRS2 cell lines
898 relative to WT cells.

899 (D) Fraction abundance of cell-cycle related proteins shown in Figure 5D depleted in
900 ΔIRS2 cell lines relative to WT cells. ΔIRS2-1 median abundance = 0.70 ; ΔIRS2-2
901 median abundance = 0.66.
902
903 ***Figure S6***: *Related to Figure 6*
904 (A) Representative frames from high-content nuclear imaging experiment for mitotic
905 fraction based on DAPI intensity. Asynchronous RPE1 WT or IRS2 KO cell lines were
906 treated with 900 nM nocodazole for 18 hours before fixing and DAPI staining.
907 (B) Asynchronous RPE1 WT or IRS2 KO cell lines were imaged every five minutes by
908 widefield time lapse microscopy for 36 hours. Each point represents an individual cell's
909 mitotic duration, measured as the time from nuclear envelope breakdown (NEB) to
910 division, slippage, or cell death. Error bars = mean ± SD. *p*-values were calculated
911 using one-way ANOVA. ns = not statistically significant.
912
913 ***Figure S7***: *Related to Figures 1-3*
914 Extended immunoblots from Figures 1, 2, and 3
915
916 ***Figure S8***: *Related to Figures 4-5*
917 Extended immunoblots from Figures 4 and 5.
918
919 ***Table S1***: APC inhibition in G_1 proteomics
920
921 ***Table S2***: Reported APC/C substrates identified by proteomics
922
923 ***Table S3***: 204 protein subset
924
925 ***Table S4***: IRS2 knockout cell proteomics
926
927
928
929

930 **References**
931

932 Alfieri, C., Zhang, S., and Barford, D. (2017). Visualizing the complex functions and
933 mechanisms of the anaphase promoting complex/cyclosome (APC/C). Open Biol *7*.

934 Besse-Patin, A., Jeromson, S., Levesque-Damphousse, P., Secco, B., Laplante, M., and
935 Estall, J.L. (2019). PGC1A regulates the IRS1:IRS2 ratio during fasting to influence
936 hepatic metabolism downstream of insulin. Proc Natl Acad Sci U S A *116*, 4285-4290.

937 Bouzakri, K., Zachrisson, A., Al-Khalili, L., Zhang, B.B., Koistinen, H.A., Krook, A., and
938 Zierath, J.R. (2006). siRNA-based gene silencing reveals specialized roles of IRS-1/Akt2
939 and IRS-2/Akt1 in glucose and lipid metabolism in human skeletal muscle. Cell Metab *4*,
940 89-96.

941 Carbon, S., Ireland, A., Mungall, C.J., Shu, S., Marshall, B., Lewis, S., Ami, G.O.H., and
942 Web Presence Working, G. (2009). AmiGO: online access to ontology and annotation
943 data. Bioinformatics *25*, 288-289.

944 Chang, L., and Barford, D. (2014). Insights into the anaphase-promoting complex: a
945 molecular machine that regulates mitosis. Curr Opin Struct Biol *29*, 1-9.

946 Chen, L., Li, Z., Ahmad, N., and Liu, X. (2015). Plk1 phosphorylation of IRS2 prevents
947 premature mitotic exit via AKT inactivation. Biochemistry *54*, 2473-2480.

948 Chirivella, L., Kirstein, M., Ferron, S.R., Domingo-Muelas, A., Durupt, F.C., Acosta-
949 Umanzor, C., Cano-Jaimez, M., Perez-Sanchez, F., Barbacid, M., Ortega, S.*, et al.*
950 (2017). Cyclin-Dependent Kinase 4 Regulates Adult Neural Stem Cell Proliferation and
951 Differentiation in Response to Insulin. Stem Cells *35*, 2403-2416.

952 Choi, B.H., Pagano, M., Huang, C., and Dai, W. (2014). Cdh1, a substrate-recruiting
953 component of anaphase-promoting complex/cyclosome (APC/C) ubiquitin E3 ligase,
954 specifically interacts with phosphatase and tensin homolog (PTEN) and promotes its
955 removal from chromatin. J Biol Chem *289*, 17951-17959.

956 Choi, E., Choe, H., Min, J., Choi, J.Y., Kim, J., and Lee, H. (2009). BubR1 acetylation at
957 prometaphase is required for modulating APC/C activity and timing of mitosis. EMBO J
958 *28*, 2077-2089.

959 Choi, E., Kikuchi, S., Gao, H., Brodzik, K., Nassour, I., Yopp, A., Singal, A.G., Zhu, H.,
960 and Yu, H. (2019). Mitotic regulators and the SHP2-MAPK pathway promote IR
961 endocytosis and feedback regulation of insulin signaling. Nature Communications *10*,
962 1473.

963 Choi, E., Zhang, X., Xing, C., and Yu, H. (2016). Mitotic Checkpoint Regulators Control
964 Insulin Signaling and Metabolic Homeostasis. Cell *166*, 567-581.

965 Clijsters, L., Ogink, J., and Wolthuis, R. (2013). The spindle checkpoint, APC/C(Cdc20),
966 and APC/C(Cdh1) play distinct roles in connecting mitosis to S phase. J Cell Biol *201*,
967 1013-1026.

968 Copps, K.D., and White, M.F. (2012). Regulation of insulin sensitivity by serine/threonine
969 phosphorylation of insulin receptor substrate proteins IRS1 and IRS2. Diabetologia *55*,
970 2565-2582.

971 Davey, N.E., and Morgan, D.O. (2016). Building a Regulatory Network with Short Linear
972 Sequence Motifs: Lessons from the Degrons of the Anaphase-Promoting Complex. Mol
973 Cell *64*, 12-23.

974 DeWard, A.D., and Alberts, A.S. (2009). Ubiquitin-mediated degradation of the formin
975 mDia2 upon completion of cell division. J Biol Chem *284*, 20061-20069.

976 Eguren, M., Alvarez-Fernandez, M., Garcia, F., Lopez-Contreras, A.J., Fujimitsu, K.,
977 Yaguchi, H., Luque-Garcia, J.L., Fernandez-Capetillo, O., Munoz, J., Yamano, H.*, et al.*
978 (2014). A synthetic lethal interaction between APC/C and topoisomerase poisons
979 uncovered by proteomic screens. Cell Rep *6*, 670-683.

980 Erickson, B.K., Mintseris, J., Schweppe, D.K., Navarrete-Perea, J., Erickson, A.R.,
981 Nusinow, D.P., Paulo, J.A., and Gygi, S.P. (2019). Active Instrument Engagement
982 Combined with a Real-Time Database Search for Improved Performance of Sample
983 Multiplexing Workflows. J Proteome Res *18*, 1299-1306.

984 Ezhevsky, S.A., Nagahara, H., Vocero-Akbani, A.M., Gius, D.R., Wei, M.C., and Dowdy,
985 S.F. (1997). Hypo-phosphorylation of the retinoblastoma protein (pRb) by cyclin D:Cdk4/6
986 complexes results in active pRb. Proc Natl Acad Sci U S A *94*, 10699-10704.

987 Folli, F., Okada, T., Perego, C., Gunton, J., Liew, C.W., Akiyama, M., D'Amico, A., La
988 Rosa, S., Placidi, C., Lupi, R.*, et al.* (2011). Altered insulin receptor signalling and beta-
989 cell cycle dynamics in type 2 diabetes mellitus. PLoS One *6*, e28050.

990 Glotzer, M., Murray, A.W., and Kirschner, M.W. (1991). Cyclin is degraded by the ubiquitin
991 pathway. Nature *349*, 132-138.

992 Haeusler, R.A., McGraw, T.E., and Accili, D. (2017). Biochemical and cellular properties
993 of insulin receptor signalling. Nature Reviews Molecular Cell Biology *19*, 31.

994 Holt, L.J. (2012). Regulatory modules: Coupling protein stability to phopshoregulation
995 during cell division. FEBS Lett *586*, 2773-2777.

996 Hornbeck, P.V., Zhang, B., Murray, B., Kornhauser, J.M., Latham, V., and Skrzypek, E.
997 (2015). PhosphoSitePlus, 2014: mutations, PTMs and recalibrations. Nucleic Acids Res
998 *43*, D512-520.

999 Huttlin, E.L., Jedrychowski, M.P., Elias, J.E., Goswami, T., Rad, R., Beausoleil, S.A.,
1000 Villen, J., Haas, W., Sowa, M.E., and Gygi, S.P. (2010). A tissue-specific atlas of mouse
1001 protein phosphorylation and expression. Cell *143*, 1174-1189.

1002 Jeng, J.C., Lin, Y.M., Lin, C.H., and Shih, H.M. (2009). Cdh1 controls the stability of
1003 TACC3. Cell Cycle *8*, 3537-3544.

1004 Ke, P.Y., Kuo, Y.Y., Hu, C.M., and Chang, Z.F. (2005). Control of dTTP pool size by
1005 anaphase promoting complex/cyclosome is essential for the maintenance of genetic
1006 stability. Genes Dev *19*, 1920-1933.

1007 Khumukcham, S.S., Samanthapudi, V.S.K., Penugurti, V., Kumari, A., Kesavan, P.S.,
1008 Velatooru, L.R., Kotla, S.R., Mazumder, A., and Manavathi, B. (2019). Hematopoietic
1009 PBX-interacting protein is a substrate and an inhibitor of the APC/C-Cdc20 complex and
1010 regulates mitosis by stabilizing cyclin B1. J Biol Chem *294*, 10236-10252.

1011 Klitzing, C., Huss, R., Illert, A.L., Froschl, A., Wotzel, S., Peschel, C., Bassermann, F.,
1012 and Duyster, J. (2011). APC/C(Cdh1)-mediated degradation of the F-box protein NIPA is
1013 regulated by its association with Skp1. PLoS One *6*, e28998.

1014 Krystkowiak, I., and Davey, N.E. (2017). SLiMSearch: a framework for proteome-wide
1015 discovery and annotation of functional modules in intrinsically disordered regions. Nucleic
1016 Acids Res *45*, W464-W469.

1017 Kubota, N., Kubota, T., Itoh, S., Kumagai, H., Kozono, H., Takamoto, I., Mineyama, T.,
1018 Ogata, H., Tokuyama, K., Ohsugi, M.*, et al.* (2008). Dynamic functional relay between
1019 insulin receptor substrate 1 and 2 in hepatic insulin signaling during fasting and feeding.
1020 Cell Metab *8*, 49-64.

1021 Lavin, D.P., White, M.F., and Brazil, D.P. (2016). IRS proteins and diabetic complications.
1022 Diabetologia *59*, 2280-2291.

1023 Lei, L., Han, F., Cui, Q., Liao, W., Liu, H., Guan, G., and Yang, L. (2018). IRS2 depletion
1024 inhibits cell proliferation and decreases hormone secretion in mouse granulosa cells. J
1025 Reprod Dev *64*, 409-416.

1026 Long, Y.C., Cheng, Z., Copps, K.D., and White, M.F. (2011). Insulin receptor substrates
1027 Irs1 and Irs2 coordinate skeletal muscle growth and metabolism via the Akt and AMPK
1028 pathways. Mol Cell Biol *31*, 430-441.

1029 Mailand, N., and Diffley, J.F. (2005). CDKs promote DNA replication origin licensing in
1030 human cells by protecting Cdc6 from APC/C-dependent proteolysis. Cell *122*, 915-926.

1031 McAlister, G.C., Nusinow, D.P., Jedrychowski, M.P., Wuhr, M., Huttlin, E.L., Erickson,
1032 B.K., Rad, R., Haas, W., and Gygi, S.P. (2014). MultiNotch MS3 enables accurate,
1033 sensitive, and multiplexed detection of differential expression across cancer cell line
1034 proteomes. Anal Chem *86*, 7150-7158.

1035 McGarry, T.J., and Kirschner, M.W. (1998). Geminin, an Inhibitor of DNA Replication, Is
1036 Degraded during Mitosis. Cell *93*, 1043-1053.

1037 Nakao, R., Hirasaka, K., Goto, J., Ishidoh, K., Yamada, C., Ohno, A., Okumura, Y.,
1038 Nonaka, I., Yasutomo, K., Baldwin, K.M.*, et al.* (2009). Ubiquitin ligase Cbl-b is a negative
1039 regulator for insulin-like growth factor 1 signaling during muscle atrophy caused by
1040 unloading. Mol Cell Biol *29*, 4798-4811.

1041 Navarrete-Perea, J., Yu, Q., Gygi, S.P., and Paulo, J.A. (2018). Streamlined Tandem
1042 Mass Tag (SL-TMT) Protocol: An Efficient Strategy for Quantitative (Phospho)proteome
1043 Profiling Using Tandem Mass Tag-Synchronous Precursor Selection-MS3. J Proteome
1044 Res *17*, 2226-2236.

1045 Prinz, S., Hwang, E.S., Visintin, R., and Amon, A. (1998). The regulation of Cdc20
1046 proteolysis reveals a role for the APC components Cdc23 and Cdc27 during S phase and
1047 early mitosis. Current Biology *8*, 750-760.

1048 Puklowski, A., Homsi, Y., Keller, D., May, M., Chauhan, S., Kossatz, U., Grunwald, V.,
1049 Kubicka, S., Pich, A., Manns, M.P.*, et al.* (2011). The SCF-FBXW5 E3-ubiquitin ligase is
1050 regulated by PLK4 and targets HsSAS-6 to control centrosome duplication. Nat Cell Biol
1051 *13*, 1004-1009.

1052 Rui, L., Yuan, M., Frantz, D., Shoelson, S., and White, M.F. (2002). SOCS-1 and SOCS-
1053 3 block insulin signaling by ubiquitin-mediated degradation of IRS1 and IRS2. J Biol Chem
1054 *277*, 42394-42398.

1055 Sackton, K.L., Dimova, N., Zeng, X., Tian, W., Zhang, M., Sackton, T.B., Meaders, J.,
1056 Pfaff, K.L., Sigoillot, F., Yu, H.*, et al.* (2014). Synergistic blockade of mitotic exit by two
1057 chemical inhibitors of the APC/C. Nature *514*, 646-649.

1058 Sakaue-Sawano, A., Kurokawa, H., Morimura, T., Hanyu, A., Hama, H., Osawa, H.,
1059 Kashiwagi, S., Fukami, K., Miyata, T., Miyoshi, H.*, et al.* (2008). Visualizing
1060 spatiotemporal dynamics of multicellular cell-cycle progression. Cell *132*, 487-498.

1061 Savitski, M.M., Wilhelm, M., Hahne, H., Kuster, B., and Bantscheff, M. (2015). A Scalable
1062 Approach for Protein False Discovery Rate Estimation in Large Proteomic Data Sets. Mol
1063 Cell Proteomics *14*, 2394-2404.

1064 Scheufele, F., Wolf, B., Kruse, M., Hartmann, T., Lempart, J., Muhlich, S., Pfeiffer, A.F.H.,
1065 Field, L.J., Charron, M.J., Pan, Z.Q.*, et al.* (2014). Evidence for a regulatory role of Cullin-
1066 RING E3 ubiquitin ligase 7 in insulin signaling. Cell Signal *26*, 233-239.

1067 Schneider, C.A., Rasband, W.S., and Eliceiri, K.W. (2012). NIH Image to ImageJ: 25
1068 years of image analysis. Nature Methods *9*, 671-675.

1069 Schweppe, D.K., Eng, J.K., Bailey, D., Rad, R., Yu, Q., Navarrete-Perea, J., Huttlin, E.L.,
1070 Erickson, B.K., Paulo, J.A., and Gygi, S.P. (2019).

1071 Seki, A., and Fang, G. (2007). CKAP2 is a spindle-associated protein degraded by
1072 APC/C-Cdh1 during mitotic exit. J Biol Chem *282*, 15103-15113.

1073 Shi, J., Luo, L., Eash, J., Ibebunjo, C., and Glass, D.J. (2011). The SCF-Fbxo40 complex
1074 induces IRS1 ubiquitination in skeletal muscle, limiting IGF1 signaling. Dev Cell *21*, 835-
1075 847.

1076 Shirakawa, J., Fernandez, M., Takatani, T., El Ouaamari, A., Jungtrakoon, P., Okawa,
1077 E.R., Zhang, W., Yi, P., Doria, A., and Kulkarni, R.N. (2017). Insulin Signaling Regulates
1078 the FoxM1/PLK1/CENP-A Pathway to Promote Adaptive Pancreatic beta Cell
1079 Proliferation. Cell Metab *25*, 868-882 e865.

1080 Singh, S.A., Winter, D., Kirchner, M., Chauhan, R., Ahmed, S., Ozlu, N., Tzur, A., Steen,
1081 J.A., and Steen, H. (2014). Co-regulation proteomics reveals substrates and mechanisms
1082 of APC/C-dependent degradation. EMBO J *33*, 385-399.

1083 Song, L., and Rape, M. (2010). Regulated degradation of spindle assembly factors by the
1084 anaphase-promoting complex. Mol Cell *38*, 369-382.

1085 Song, M.S., Carracedo, A., Salmena, L., Song, S.J., Egia, A., Malumbres, M., and
1086 Pandolfi, P.P. (2011). Nuclear PTEN regulates the APC-CDH1 tumor-suppressive
1087 complex in a phosphatase-independent manner. Cell *144*, 187-199.

1088 Sun, X.J., Wang, L.M., Zhang, Y., Yenush, L., Myers, M.G., Jr., Glasheen, E., Lane, W.S.,
1089 Pierce, J.H., and White, M.F. (1995). Role of IRS-2 in insulin and cytokine signalling.
1090 Nature *377*, 173-177.

1091 Wan, Y., Liu, X., and Kirschner, M.W. (2001). The Anaphase-Promoting Complex
1092 Mediates TGF-β Signaling by Targeting SnoN for Destruction. Molecular Cell *8*, 1027-
1093 1039.

1094 Wang, H., Liu, D., Wang, Y., Qin, J., and Elledge, S.J. (2001). Pds1 phosphorylation in
1095 response to DNA damage is essential for its DNA damage checkpoint function. Genes
1096 Dev *15*, 1361-1372.

1097 Wu, S., Zhou, B., Xu, L., and Sun, H. (2009). IRS-2, but not IRS-1, can sustain
1098 proliferation and rescue UBF stabilization in InR or InR defective signaling of 32D myeloid
1099 cells. Cell Cycle *8*, 3218-3226.

1100 Xu, X., Sarikas, A., Dias-Santagata, D.C., Dolios, G., Lafontant, P.J., Tsai, S.C., Zhu, W.,
1101 Nakajima, H., Nakajima, H.O., Field, L.J.*, et al.* (2008). The CUL7 E3 ubiquitin ligase
1102 targets insulin receptor substrate 1 for ubiquitin-dependent degradation. Mol Cell *30*, 403-
1103 414.

1104 Yi, J.S., Park, J.S., Ham, Y.M., Nguyen, N., Lee, N.R., Hong, J., Kim, B.W., Lee, H., Lee,
1105 C.S., Jeong, B.C.*, et al.* (2013). MG53-induced IRS-1 ubiquitination negatively regulates
1106 skeletal myogenesis and insulin signalling. Nat Commun *4*, 2354.

1107 Zeng, X., Sigoillot, F., Gaur, S., Choi, S., Pfaff, K.L., Oh, D.C., Hathaway, N., Dimova, N.,
1108 Cuny, G.D., and King, R.W. (2010). Pharmacologic inhibition of the anaphase-promoting
1109 complex induces a spindle checkpoint-dependent mitotic arrest in the absence of spindle
1110 damage. Cancer Cell *18*, 382-395.

1111 Zhang, P.J., Zhao, J., Li, H.Y., Man, J.H., He, K., Zhou, T., Pan, X., Li, A.L., Gong, W.L.,
1112 Jin, B.F.*, et al.* (2007). CUE domain containing 2 regulates degradation of progesterone
1113 receptor by ubiquitin-proteasome. EMBO J *26*, 1831-1842.

1114 Zhang, W.N., Zhou, J., Zhou, T., Li, A.L., Wang, N., Xu, J.J., Chang, Y., Man, J.H., Pan,
1115 X., Li, T.*, et al.* (2013). Phosphorylation-triggered CUEDC2 degradation promotes UV-
1116 induced G1 arrest through APC/C(Cdh1) regulation. Proc Natl Acad Sci U S A *110*,
1117 11017-11022.
1118
1119
1120
1121
1122
1123

Figure 1

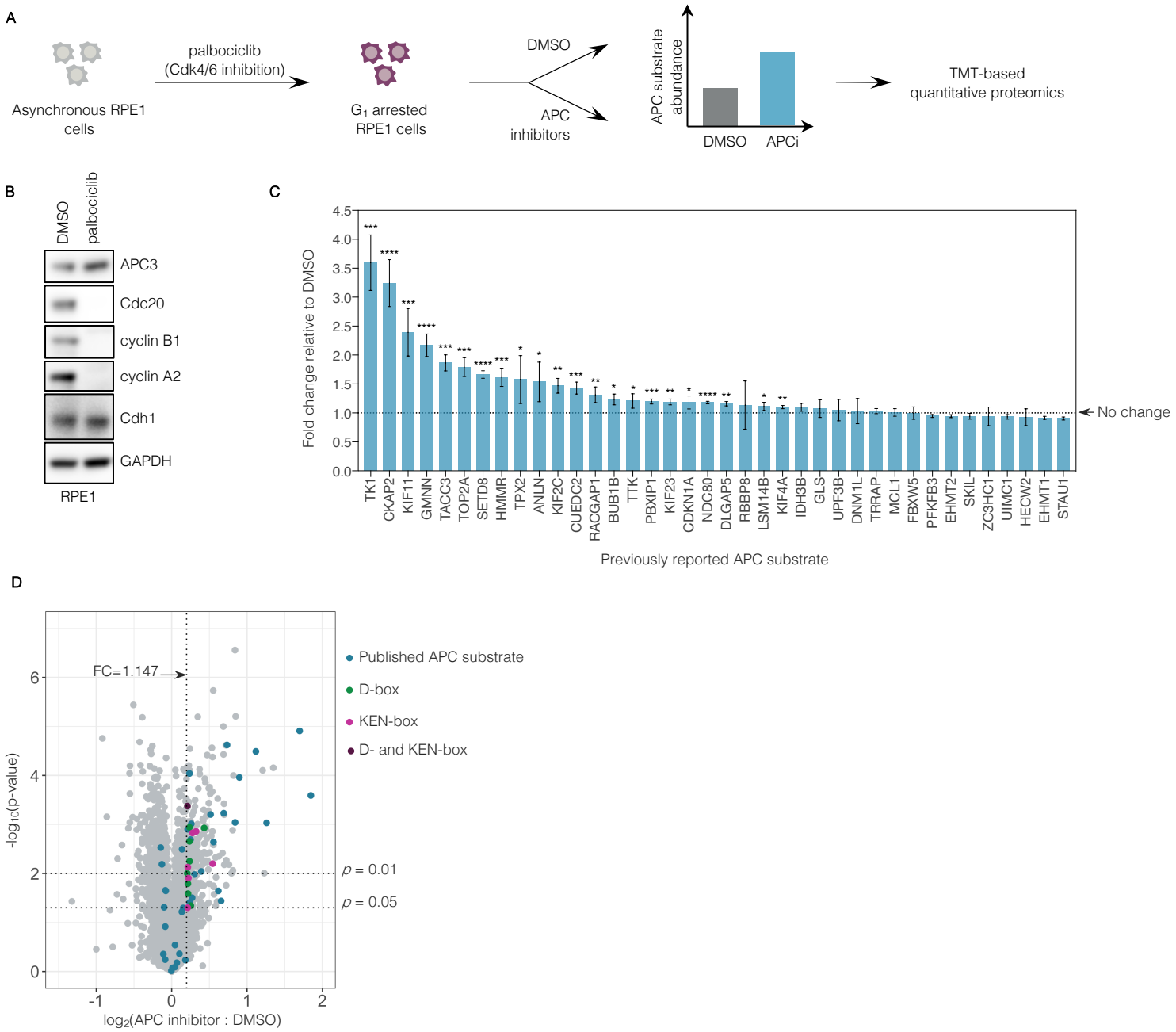
A
Asynchronous RPE1 cells
palbociclib (Cdk4/6 inhibition)
G1 arrested RPE1 cells
DMSO
APC inhibitors
APC substrate abundance
DMSO
APCi
TMT-based quantitative proteomics
B
DMSO
palbociclib
APC3
Cdc20
cyclin B1
cyclin A2
Cdh1
GAPDH
RPE1
C
Fold change relative to DMSO
No change
TK1
CKAP2
KIF11
GMNN
TACC3
TOP2A
SETD8
HMMR
TPX2
ANLN
KIF2C
CUEDC2
RACGAP1
BUB1B
TTK
PBXIP1
KIF23
CDKN1A
NDC80
DLGAP5
RBBP8
LSM14B
KIF4A
IDH3B
GLS
UPF3B
DNM1L
TRRAP
MCL1
FBXW5
PFKFB3
EHMT2
SKIL
ZC3HC1
UIMC1
HECW2
EHMT1
STAU1
Previously reported APC substrate
D
FC=1.147
Published APC substrate
D-box
KEN-box
D- and KEN-box
p = 0.01
p = 0.05
-log10(p-value)
log2(APC inhibitor : DMSO)

Figure 2

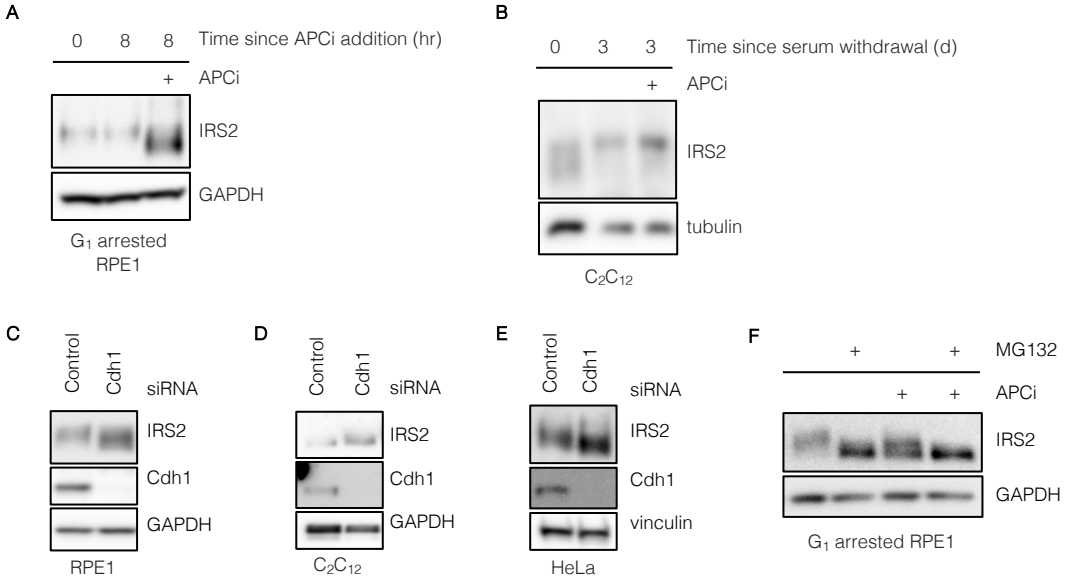
A
0
8
8
Time since APCi addition (hr)
+
APCi
IRS2
GAPDH
G1 arrested
RPE1
B
0
3
3
Time since serum withdrawal (d)
+
APCi
IRS2
tubulin
C2C12
C
Control
Cdh1
siRNA
IRS2
Cdh1
GAPDH
RPE1
D
Control
Cdh1
siRNA
IRS2
Cdh1
GAPDH
C2C12
E
Control
Cdh1
siRNA
IRS2
Cdh1
vinculin
HeLa
F
+
+
MG132
+
+
APCi
IRS2
GAPDH
G1 arrested RPE1

Figure 3

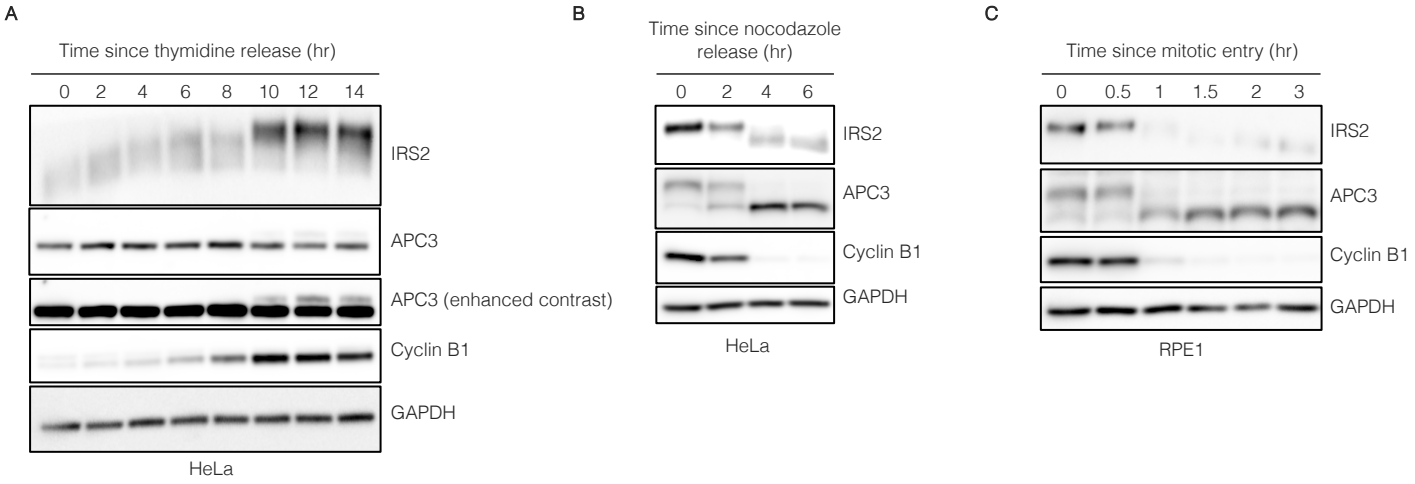
A
Time since thymidine release (hr)
0 2 4 6 8 10 12 14
IRS2
APC3
APC3 (enhanced contrast)
Cyclin B1
GAPDH
HeLa
B
Time since nocodazole release (hr)
0 2 4 6
IRS2
APC3
Cyclin B1
GAPDH
HeLa
C
Time since mitotic entry (hr)
0 0.5 1 1.5 2 3
IRS2
APC3
Cyclin B1
GAPDH
RPE1

Figure 4

A

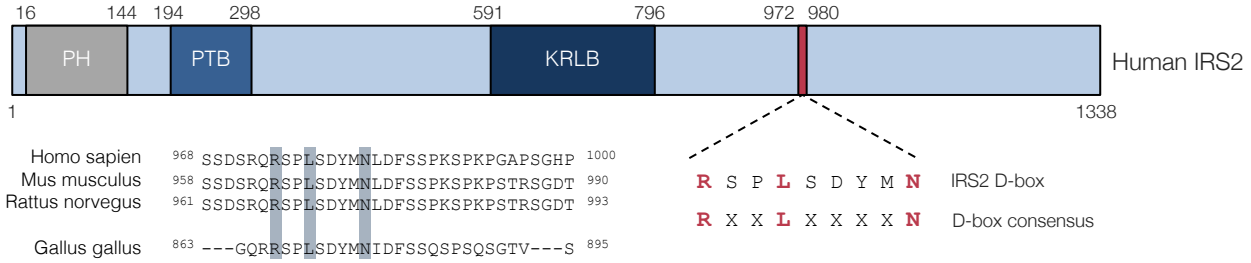

B

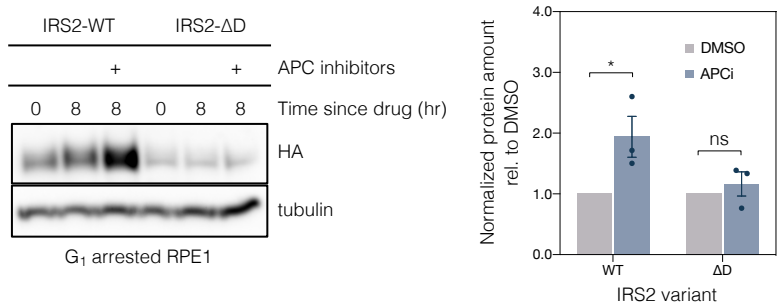

D

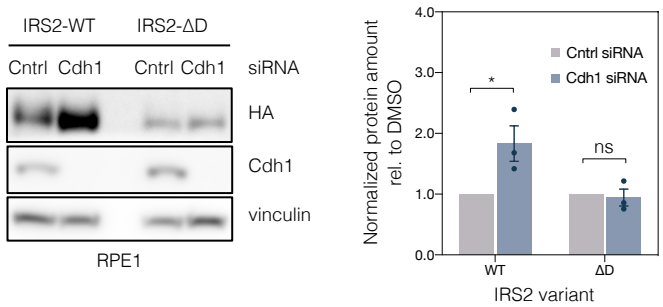

C

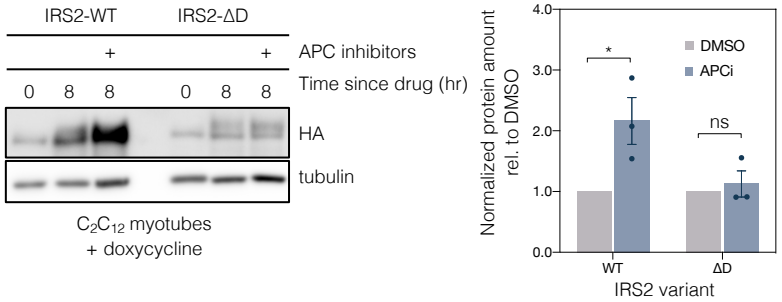

E

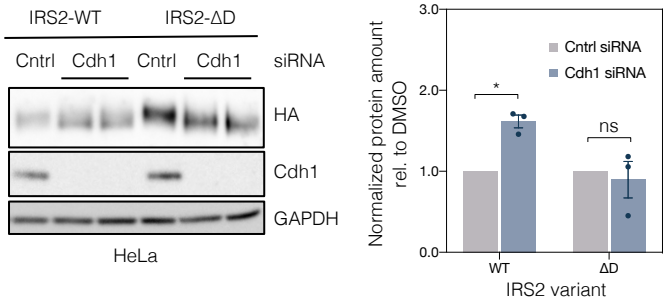

F

G

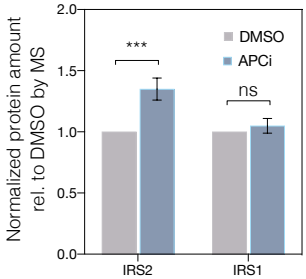

H

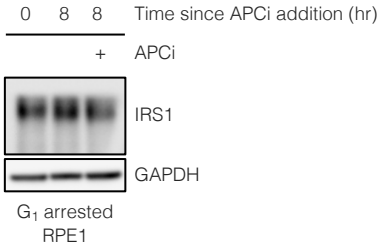

I

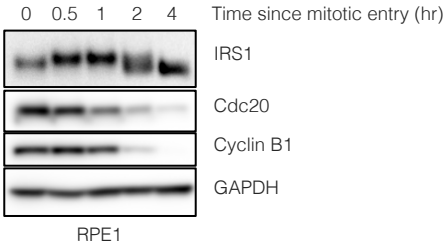

Figure 5

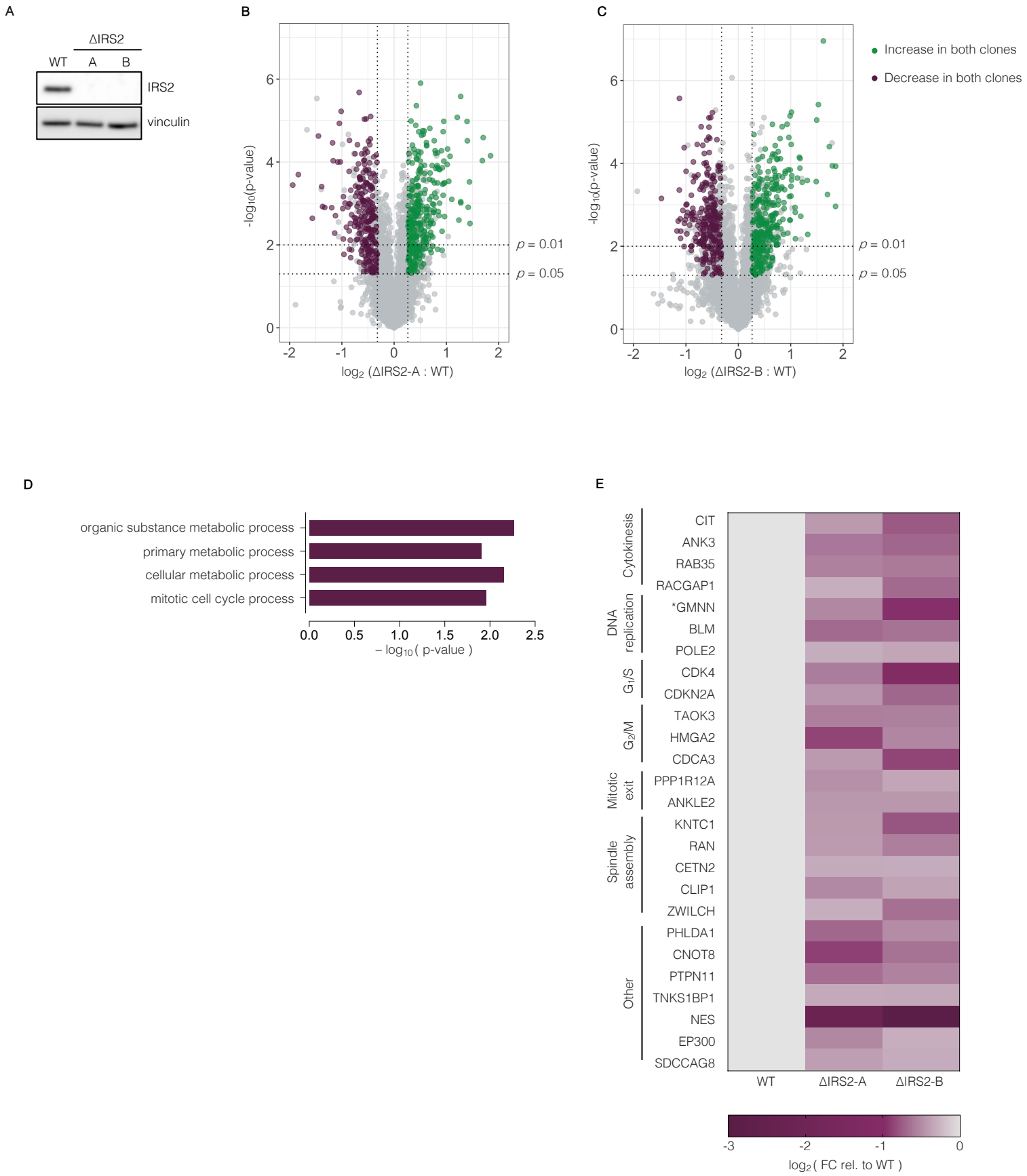
A
ΔIRS2
WT
A
B
IRS2
vinculin
B
-log10(p-value)
log2 (ΔIRS2-A : WT)
p = 0.01
p = 0.05
C
Increase in both clones
Decrease in both clones
-log10(p-value)
log2 (ΔIRS2-B : WT)
p = 0.01
p = 0.05
D
organic substance metabolic process
primary metabolic process
cellular metabolic process
mitotic cell cycle process
– log10(p-value)
E
Cytokinesis
CIT
ANK3
RAB35
RACGAP1
DNA replication
*GMNN
BLM
POLE2
G1/S
CDK4
CDKN2A
G2/M
TAOK3
HMGA2
CDCA3
Mitotic exit
PPP1R12A
ANKLE2
Spindle assembly
KNTC1
RAN
CETN2
CLIP1
ZWILCH
Other
PHLDA1
CNOT8
PTPN11
TNKS1BP1
NES
EP300
SDCCAG8
WT
ΔIRS2-A
ΔIRS2-B
log2(FC rel. to WT)

Figure 6

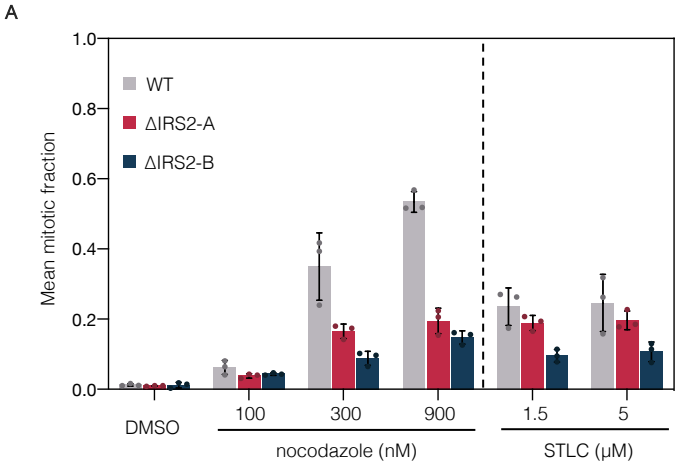
A
Mean mitotic fraction
1.0
0.8
0.6
0.4
0.2
0.0
WT
ΔIRS2-A
ΔIRS2-B
DMSO
100
300
900
1.5
5
nocodazole (nM)
STLC (μM)

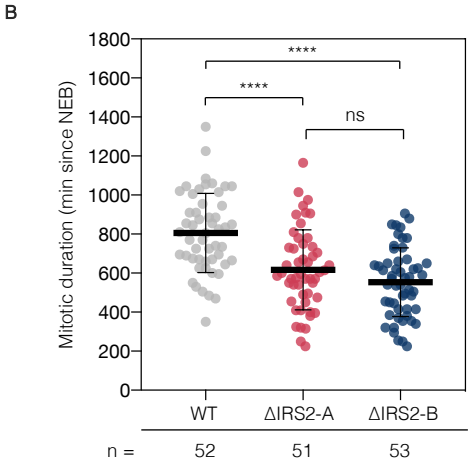
B
Mitotic duration (min since NEB)
1800
1600
1400
1200
1000
800
600
400
200
0
****
****
ns
WT
ΔIRS2-A
ΔIRS2-B
n =
52
51
53

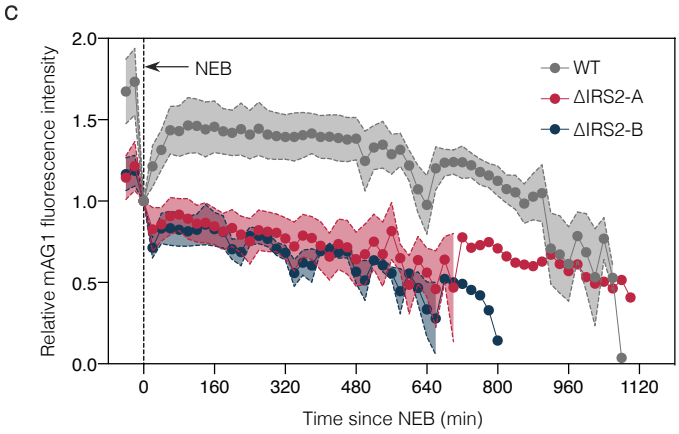
C
Relative mAG1 fluorescence intensity
2.0
1.5
1.0
0.5
0.0
NEB
WT
ΔIRS2-A
ΔIRS2-B
0
160
320
480
640
800
960
1120
Time since NEB (min)

Figure 7

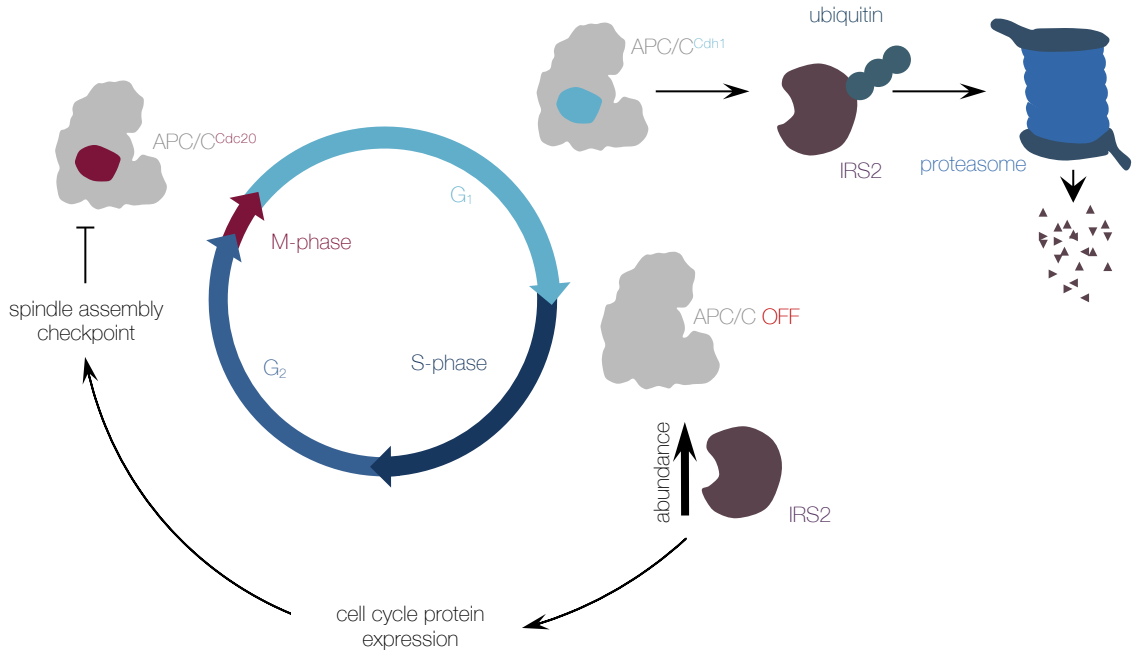
APC/C^{Cdc20}
spindle assembly
checkpoint
M-phase
G_1
S-phase
G_2
APC/C^{Cdh1}
ubiquitin
IRS2
proteasome
APC/C OFF
abundance
IRS2
cell cycle protein
expression